Tectonics®

RESEARCH ARTICLE
10.1029/2023TC007956

Key Points:

- Shortening up to 2 mm/yr suggests activity of the Ventas de Zafarraya normal Fault simultaneous to folding
- The Sierra de Alhama-Zafarraya Polje area belongs to a compressional front located to the W and SW of the extensional Granada Basin
- Shallow normal faults may constitute the surface expression of deep main faults developed in a complex crustal compressional setting

Supporting Information:

Supporting Information may be found in the online version of this article.

Correspondence to:

A. Madarieta-Txurruka and L. González-Castillo,
amadatxu@ugr.es;
lgcastillo@ugr.es

Citation:

Madarieta-Txurruka, A., González-Castillo, L., Peláez, J. A., Galindo-Zaldívar, J., Borque, M. J., Lacy, M. C., et al. (2024). Active shortening simultaneous to normal faulting based on GNSS, geophysical, and geological data: The seismogenic Ventas de Zafarraya Fault (Betic Cordillera, southern Spain). *Tectonics*, *43*, e2023TC007956. https://doi.org/10.1029/2023TC007956

Received 7 JUN 2023
Accepted 4 JAN 2024

Author Contributions:

Conceptualization: Asier Madarieta-Txurruka, Lourdes González-Castillo, José A. Peláez, Jesús Galindo-Zaldívar, Antonio J. Gil

Active Shortening Simultaneous to Normal Faulting Based on GNSS, Geophysical, and Geological Data: The Seismogenic Ventas de Zafarraya Fault (Betic Cordillera, Southern Spain)

Asier Madarieta-Txurruka[1], Lourdes González-Castillo[1], José A. Peláez[2], Jesús Galindo-Zaldívar[1,3], María J. Borque[4,5], María C. Lacy[4,5], Antonio M. Ruiz-Armenteros[4,5], Jesús Henares[6], Patricia Ruano[1,3], Alberto Sánchez-Alzola[7], Manuel Avilés[4], Gracia Rodríguez-Caderot[8], Francisco José Martínez-Moreno[9], Víctor Tendero-Salmerón[1,3], Raquel Vinardell-Peña[4], and Antonio J. Gil[4,5]

[1]Departamento de Geodinámica, Universidad de Granada, Granada, Spain, [2]Departamento de Física, Universidad de Jaén, Jaén, Spain, [3]Instituto Andaluz de Ciencias de la Tierra (CSIC-UGR), Granada, Spain, [4]Departamento Ing. Cartográfica, Geodésica y Fotogrametría, Universidad de Jaén, Jaén, Spain, [5]Centro de Estudios Avanzados en Ciencias de la Tierra, Energía y Medio Ambiente (CEACTEMA), Universidad de Jaén, Jaén, Spain, [6]Universidad Internacional de La Rioja, Logroño, Spain, [7]Departamento de Estadística e Investigación Operativa, Universidad de Cádiz, Puerto Real, Spain, [8]Departamento de Física de la Tierra y Astrofísica, Universidad Complutense de Madrid, Madrid, Spain, [9]Departamento de Geodinámica, Paleontología y Estratigrafía, Universidad Complutense de Madrid, Madrid, Spain

Abstract The central Betic Cordillera, southern Spain, is affected by an uplift related to the NNW–SSE Eurasia-Nubia convergence and shallow ENE–WSW orthogonal extension accommodated by the extensional system of the Granada Basin. The combination of geophysical, geodetic, and geological data reveals that the southwestern boundary of this extensional system is a seismically active compressional front extending from the W to the SW of the Granada Basin. The near-field Global Navigation Satellite System data determine NNE–SSW shortening of up to 2 mm/yr of the compressional front in the Zafarraya Polje. In this setting, the normal Ventas de Zafarraya Fault developed as a result of the bending-moment extension of the Sierra de Alhama antiform and was last reactivated during the 1884 Andalusian earthquake (Mw 6.5). The uplift in the central Betic Cordillera together with the subsidence in the Western Alborán Basin may facilitate a westward to southwestward gravitational collapse through the extensional detachment of the Granada Basin. The heterogeneous crust of the Betic Cordillera would generate the compressional front, which is divided into two sectors: thrusting to the west, and folding associated with buttressing to the south. Our results evidence that basal detachments, linking extensional fault activity with compressional fronts, may determine the activity of local surface structures and the geological hazard in densely populated regions.

Plain Language Summary A combination of geological, geophysical, and geodetic methods is used to understand the evolution in the frontal area of the extensional system of Granada Basin, near the Zafarraya Polje. In particular, this approach improves our knowledge of the Ventas de Zafarraya Fault (VZF) that hosted the 1884 Andalusian earthquake. Seismic data provide information on the distribution of stress and deformation in the region and made it possible to identify a compressional front linked to the extensional system of the Granada Basin. Global Navigation Satellite System (GNSS) data accurately locate the sites of the Zafarraya GNSS network surrounding the VZF, and repeated measurements provide deformation rates of the area that suggests shortening. Thus, we locate the VZF within the former compressional setting. Meanwhile, electrical-resistivity tomography images sub-surface structures given its electrical properties and, together with the field geological observations, suggests the extensional behavior of the fault. Therefore, it is considered to be a fold-related fault formed due to the extension of the outer arc of the Sierra de Alhama antiform. As in the research presented here, a joint interpretation of data from different methods makes it possible to propose active seismic tectonic extensional models in a compressional setting applicable to other regions.

1. Introduction

Active normal faults are brittle structures accommodating deformation in regions affected by extension (e.g., Jackson, 1987; Jackson & White, 1989). However, in active orogenic belts developed by shortening, most of the normal faults accommodate regional orthogonal extension (e.g., in metamorphic core complexes, Rey et al., 2017;

Data curation: Asier Madarieta-Txurruka, Lourdes González-Castillo, José A. Peláez, Jesús Galindo-Zaldívar, María J. Borque, María C. Lacy, Antonio M. Ruiz-Armenteros, Jesús Henares, Patricia Ruano, Alberto Sánchez-Alzola, Manuel Avilés, Gracia Rodríguez-Caderot, Francisco José Martínez-Moreno, Víctor Tendero-Salmerón, Raquel Vinardell-Peña, Antonio J. Gil
Formal analysis: Asier Madarieta-Txurruka, Lourdes González-Castillo, José A. Peláez, Jesús Galindo-Zaldívar, María J. Borque, María C. Lacy, Antonio M. Ruiz-Armenteros, Jesús Henares, Patricia Ruano, Alberto Sánchez-Alzola, Manuel Avilés, Gracia Rodríguez-Caderot, Francisco José Martínez-Moreno, Víctor Tendero-Salmerón, Raquel Vinardell-Peña, Antonio J. Gil
Funding acquisition: José A. Peláez, Jesús Galindo-Zaldívar, Antonio J. Gil
Investigation: Asier Madarieta-Txurruka, Lourdes González-Castillo, José A. Peláez, Jesús Galindo-Zaldívar, María J. Borque, María C. Lacy, Antonio M. Ruiz-Armenteros, Jesús Henares, Patricia Ruano, Alberto Sánchez-Alzola, Manuel Avilés, Gracia Rodríguez-Caderot, Francisco José Martínez-Moreno, Víctor Tendero-Salmerón, Raquel Vinardell-Peña, Antonio J. Gil
Methodology: Asier Madarieta-Txurruka, Lourdes González-Castillo, José A. Peláez, Jesús Galindo-Zaldívar, Antonio J. Gil
Project Administration: José A. Peláez, Jesús Galindo-Zaldívar, Antonio J. Gil
Resources: José A. Peláez, Jesús Galindo-Zaldívar, María J. Borque, María C. Lacy, Antonio M. Ruiz-Armenteros, Jesús Henares, Manuel Avilés, Antonio J. Gil
Software: José A. Peláez, Jesús Galindo-Zaldívar, Antonio J. Gil
Supervision: Lourdes González-Castillo, José A. Peláez, Jesús Galindo-Zaldívar, Antonio J. Gil
Validation: Lourdes González-Castillo, José A. Peláez, Jesús Galindo-Zaldívar, Antonio J. Gil
Visualization: Asier Madarieta-Txurruka, José A. Peláez, Jesús Galindo-Zaldívar, Antonio J. Gil
Writing – original draft: Asier Madarieta-Txurruka, Lourdes González-Castillo, Jesús Galindo-Zaldívar, Antonio J. Gil
Writing – review & editing: Lourdes González-Castillo, José A. Peláez, Jesús Galindo-Zaldívar, María J. Borque, María C. Lacy, Antonio M. Ruiz-Armenteros, Jesús Henares, Patricia Ruano, Alberto Sánchez-Alzola, Manuel Avilés, Gracia Rodríguez-Caderot, Francisco José Martínez-Moreno, Víctor Tendero-Salmerón, Raquel Vinardell-Peña, Antonio J. Gil

Searle & Lamont, 2020) or local extension parallel to regional shortening, as occurs in folds (Galindo-Zaldívar et al., 2003; Li et al., 2018; Stephenson et al., 2007; Yeats et al., 1981).

The extension in orogenic belts is related to or can be intensified by gravitational collapse processes (e.g., England & Houseman, 1989; England & Molnar, 1997; Flesch et al., 2000; Morley, 2007; Rey et al., 2010). Shortening involves thickening of the crust, uplift of the relief, and, finally, destabilization of the uplifted areas. Consequently, the elevated regions are affected by thinning and extension, while the surrounding crust may be influenced by thickening if there is any fixed boundary (Selverstone, 2005). Regionally, these processes may be restricted to the upper crust or even to involve whole the crust (Rey et al., 2001). When extension affects only the upper crust, normal faults occur above an extensional detachment developed in the thickest part of the crust. The detachment is connected with thrusts in the surrounding and frontal areas, sometimes reaching the foreland (e.g., Mancktelow & Pavlis, 1994; Rey et al., 2011; Wdowinski & Axen, 1992). The geometry of these thrust systems will also depend on the crustal structure beneath the detachment, determining the formation of lateral and oblique ramps (Boyer, 1995; Hinsch et al., 2002; Mitra, 1997; Wiltschko & Eastman, 1983). In fact, one of the most important control mechanisms for the geometry of thrust systems is active buttressing (Woodward, 1988). The migration of extensional systems is another factor to consider in gravitational collapse and thrusting phenomena. In these systems, the activity is not always distributed uniformly over time but migrates from some faults to others (e.g., Buck, 1988; Goldsworthy & Jackson, 2001; Gresseth et al., 2023; Wallace, 1987). This active migration likewise affects the evolution of the thrust front, pushing it to propagate in the same trend. Overall, thrusting generally migrates from the inner part toward the outer part of the orogen (Zhao et al., 2022) and develops a piggyback mode of propagation (e.g., Fillon et al., 2013; Ghani et al., 2021; Jia et al., 2020; Ori & Friend, 1984).

Gravitational collapse is characterized by the interaction of faults and folds. There are folds formed by fault activity (Brandes & Tanner, 2014) and faults formed by fold activity (Yeats et al., 1981). Fold-related extensional fractures (Cosgrove, 2015; Nabavi & Fossen, 2021) can develop perpendicular, oblique, or parallel to the fold axis (Stephenson et al., 2007), thereby providing insight into the relationship between strain and stress (Amrouch et al., 2010; Silliphant et al., 2002). Orthogonal and oblique-to-fold-axis fractures accommodate extension perpendicular to shortening (Moustafa, 2013), while parallel fractures are related to bending-moment extension in the outer arc (Yeats et al., 1981). These fractures sometimes constitute well-developed faults, whose main features will depend on the fold type (Li et al., 2018; Livio et al., 2019; Yeats et al., 1981). Faulting thus depends on fold symmetry, interlimb angle, curvature intensity (Watkins et al., 2018), and lithological and stratigraphic features (Li et al., 2018), among others. The seismic activity of such faults has not been studied in detail, although in certain cases historical events have been correlated with earthquakes occurring on basal thrust systems (Meghraoui & Doumaz, 1996).

The interaction between faults and folds can be studied using near-field Global Navigation Satellite System (GNSS) networks (Tsukahara & Takada, 2018). These networks consist of measurements taken near structures that are suspected to be active (Keller & Pinter, 1996). They allow for quantifying the shortening and lengthening of the Earth's surface on a local scale and to compare geodetic slip rates with present-day fault kinematics and faulting and folding rates obtained from geological observations (Galindo-Zaldívar et al., 2022). On the other hand, regional scale processes such as orogenic building and dismantling (e.g., Bilham et al., 1997; Niemi et al., 2004; Nocquet et al., 2016) and plate motion (Kreemer et al., 2014) can be investigated using a far-field approach, which involves measurements over long distances, far away from any specific active structure (Keller & Pinter, 1996). Furthermore, these networks can also serve to estimate fault slip rates of specific structures, if the site configuration adequately covers them. Precise Point Positioning (PPP) (Zumberge et al., 1997) is one of the available GNSS processing methods for quantifying geodynamic processes causing deformation on the scale of mm/yr (Hreinsdóttir et al., 2006; Kouba, 2005; Larson et al., 2004; Smith et al., 2004), which is very important in regions with low deformation rates.

The Betic Cordillera, southern Spain (Figure 1), is a key region for studying interactions between extensional and compressional structures, hence the interaction between normal faulting and folding. This cordillera is the northern branch of the Gibraltar Arc, the westernmost alpine belt in the Mediterranean that also includes the Rif Cordillera constituting the southern branch. The Betic Cordillera is composed of two domains divided by Flysch Units (Fontboté & Estévez, 1980) (Figure 1a). The Internal Zones, in the south, are mainly formed by three superimposed metamorphic complexes (Nevado-Filábride, Alpujárride, and Maláguide) (Fallot, 1948). The External Zones, to the north, constitute the thrust-and-fold belt formed by Meso-Cenozoic rocks of the South-Iberian paleomargin (Balanyá & García-Dueñas, 1987). There are Neogene-Quaternary intramontane basins within the

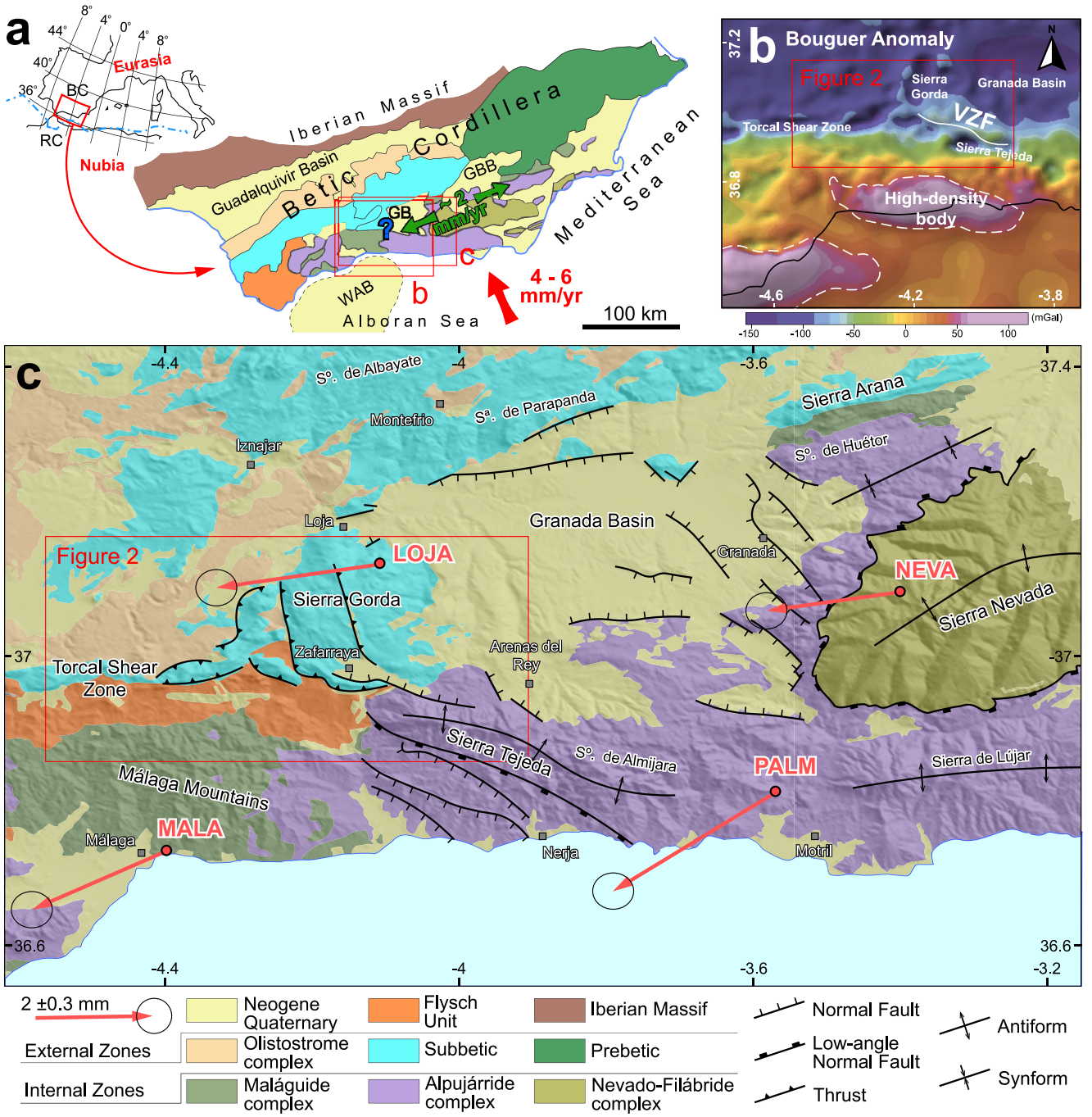

Figure 1. Geological and tectonic setting of the central Betic Cordillera: (a) Geological sketch of the Betic Cordillera. The red arrow indicates a motion of Nubia relative to stable Eurasia from DeMets et al. (2010), McClusky et al. (2003), and Nocquet and Calais (2003). Green arrows indicate a WSW–ENE extension registered in the central Betic Cordillera from Galindo-Zaldívar et al. (2015), Palano et al. (2015), and Serpelloni et al. (2007). WAB: Western Alborán Basin. GB: Granada Basin. GBB: Guadix-Baza Basin. (b) Bouguer anomaly map derived from free-air anomaly data (Sandwell et al., 2013). (c) Simplified geological map of the central Betic Cordillera modified from Rodríguez et al. (2015), Ruano et al. (2004), and Galindo-Zaldívar et al. (2000). Red arrows represent the Global Navigation Satellite System data taken from Galindo-Zaldívar et al. (2015). The position of the study area shown in Figure 2 is indicated in (b) and (c).

Betic Cordillera, with some of them, like the Granada Basin and the Zafarraya Polje, situated along the Internal/External Zones boundary.

Recent models explaining the evolution of Betic Cordillera can be summarized in two main groups: (a) delamination of the Alborán lithospheric mantle (e.g., Calvert et al., 2000; Houseman et al., 1981; Platt & Vissers, 1989;

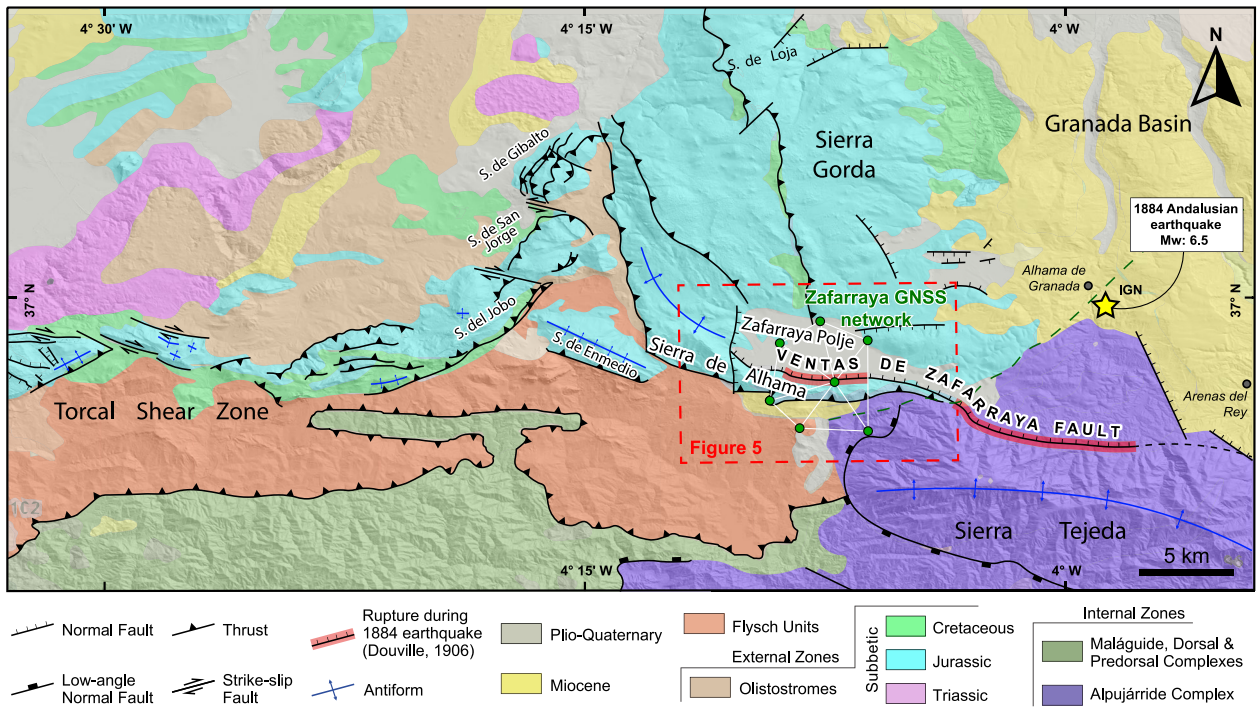

Figure 2. Geological and tectonic map of the study area modified from Rodríguez et al. (2015). The green dots and the dashed white lines represent the Zafarraya survey mode Global Navigation Satellite System network. The yellow star represents the epicenter of the 1884 Andalusian earthquake (National Geographic Institute, 2023). The red line box shows the location of Figure 5.

Seber et al., 1996), and (b) subduction beneath the Alborán Domain with or without rollback/slab tearing (e.g., Blanco & Spakman, 1993; Chertova et al., 2014; Garcia-Castellanos & Villaseñor, 2011; González-Castillo et al., 2015a; Mancilla et al., 2015; Pedrera et al., 2011; Ruiz-Constán et al., 2011).

The main deformation in the Betic Cordillera was the large dextral displacement between the Internal and External zones from the Cretaceous until at least the middle Miocene (Sanz de Galdeano, 1990). Subsequently, the Betic Cordillera was affected by a N–S to NNW–SSE compression due to the Eurasia-Nubia convergence (Braga et al., 2003; Sanz de Galdeano & Alfaro, 2004). This convergence has produced uplift and perpendicular extension in the central sector of Internal Zones since the middle Miocene (Braga et al., 2003; Perez-Peña et al., 2010; Reinhardt et al., 2007). The extension allows for the exhumation of metamorphic complexes due to the formation of WSW-directed and west-dipping low-angle normal faults, such as the Mecina detachment in Sierra Nevada (Galindo-Zaldívar et al., 1989; Jabaloy et al., 1993).

The Betic Cordillera is currently affected by a NNW–SSE to NW–SE 4–6 mm/yr Eurasia-Nubia convergence (DeMets et al., 2010; McClusky et al., 2003; Nocquet & Calais, 2003). At the same time, a nearly 2 mm/yr ENE–WSW extension perpendicular to regional compression occurs in the central Betic Cordillera (Galindo-Zaldívar et al., 2015; Martín-Rojas et al., 2023; Palano et al., 2015; Serpelloni et al., 2007), forming active high- and low-angle normal faults (Galindo-Zaldívar et al., 1999; Lozano et al., 2022; Madarieta-Txurruka et al., 2021, 2022; Sanz de Galdeano et al., 2003). Today, the Granada Basin is the main extensional active basin of the central Betic Cordillera (Morales et al., 1990; Rodríguez-Fernández & Sanz de Galdeano, 2006). It is affected by low-to-moderate recurrent seismicity in its eastern part (Galindo-Zaldívar et al., 1999) related to NW–SE striking normal faulting that indicates W–E to NE–SW extension (Madarieta-Txurruka et al., 2021). This sector is also affected by perpendicular NE–SW striking normal faults (Madarieta-Txurruka et al., 2022) and microfaults also evidencing radial extension in the region (Galindo-Zaldívar et al., 1999). In addition, GNSS data available for the region (Galindo-Zaldívar et al., 2015; Gil et al., 2017) point to an extension that rotates and decreases in rate from E–W in the north to NE–SW in the south (Madarieta-Txurruka et al., 2022).

To the west (Figure 1b), the evolution of this extensional system is unclear, but the area is also affected by compressional and strike-slip deformation. The northwestern part of the Granada Basin has undergone NW–

SE compression, as indicated by WSW–ENE striking folds affecting Turolian rocks and striated pebbles of Languian-Burdingalian to Plio-Quaternary age rocks (Ruano, 2003). Sierra Gorda, to the west, is characterized by thrusts and folds (Elorza et al., 1978; Sanz de Galdeano, 2013) indicating WSW displacement during the Miocene, probably linked to the low-angle normal faults of eastern Granada Basin, likewise active during the Miocene (Galindo-Zaldívar et al., 2000). To the south, east of the Zafarraya Polje, Pliocene-Pleistocene striated pebbles indicate a NNW–SSE and W–E Quaternary compression (Sanz de Galdeano, 1985). Finally, the Sierra Tejeda Antiform is the main structure bounding the Granada Basin to the SW. This antiform is currently uplifting, as evidenced by a highly incised drainage network (Ruano et al., 2004). It strikes W–E and bends to WNW–ESE in the western part. The southern limb is affected by normal-to-normal-dextral low-angle normal faults, in turn related to the exhumation of metamorphic core complexes during the Miocene (Fernández Fernández et al., 1992), that are folded and sealed by Quaternary sediments (Ruano, 2003). Bouguer Anomaly data available for the region (Ayala et al., 2016; Torné et al., 1992) show two main positive anomalies located along the coast of Málaga, west of Sierra Tejeda (Figure 1c). Those anomalies have been associated with ultramafic rocks embedded in the crust (Pedrera et al., 2020; Torne et al., 1992).

The GNSS data show a general displacement to the W–SW with respect to stable Iberia (Figure 1b) and ENE–WSW shortening (Galindo-Zaldívar et al., 2015; Martín-Rojas et al., 2023), consistent with geological evidence of compression at the western and southwestern boundaries of the Granada Basin. Seismological data west of the Granada Basin differ providing earthquake focal mechanisms (EFMs) not only of compressional faulting, but also of strike-slip and normal faulting. The strike-slip earthquakes sited in the northern part of Sierra Gorda indicate both N–S sinistral and W–E dextral behavior (Carmona et al., 2009; Stich et al., 2003). The Sierra Gorda and other mountain ranges located to the west are mainly characterized by strike-slip and normal faulting EFMs, but compressional faulting also occurs (Balanyá et al., 2012). Toward the south, seismicity decreases drastically and no EFMs are available.

The Zafarraya Polje (Figure 2) is located southwest of the Granada Basin, between Sierra Gorda and Sierra Tejeda. It is an endorheic basin consisting of a plain and several ponors where water infiltrates into the ground, as is common for poljes. However, its formation is due to erosion and tectonic processes rather than karst. It is bounded by normal faults, but lies between folds and reverse faults (Sanz de Galdeano, 2013). The Ventas de Zafarraya Fault (VZF) is the main active seismogenic normal fault in the region (Grützner et al., 2013; Reicherter et al., 2003). Yet Galindo-Zaldívar et al. (2003) and Ruano et al. (2004) consider a secondary structure of the region, related to the extension of the outer arc of Sierra de Alhama and Sierra Tejeda folds affecting both the Internal and External Zones. This fault has been linked to the 1884 Andalusian earthquake (Mudarra-Hernández et al., 2023; Reicherter et al., 2003), one of the most important historical earthquakes in the Iberian Peninsula (Mezcua et al., 2004; Udías & Muñoz, 1979). It has been linked to normal faulting (Reicherter et al., 2003), reaching intensity IX-X (EMS-98 scale), and an estimated magnitude equal to Mw 6.5 (Mezcua et al., 2004). The hypocenter is located between Alhama de Granada and Arenas del Rey (Figure 2) (Martinez Solares & Mezcua, 2002), at a depth of about 10–20 km (Udías & Muñoz, 1979). Further faults strike E–W, NE–SW, and N–S, as the West Polje Fault (Sanz de Galdeano, 2013).

This study aims to quantify the deformation in the Zafarraya Polje area, where the normal seismogenic VZF lies, providing new insights regarding the development of this extensional structure in the context of the active evolution of the Betic Cordillera collisional alpine belt. This multidisciplinary study combines geophysical, geodetic, and geological analyses. New data presented include the Zafarraya survey mode GNSS network, relocated seismicity in the western and southwestern boundaries of the Granada Basin, electrical-resistivity tomography (ERT) profiles, and new structural and kinematic data. Our results may contribute to a better understanding of extensional fault systems in orogens, whose activity represents a seismic hazard for nearby populations.

2. Data and Methods

This multidisciplinary study integrates seismological, GNSS, geological data, and ERT profiles. The seismological data consist of relocated seismicity occurring in the area since 2000, compilation of the available EFMs solutions, and calculation of stress tensors in the region comprised between −4.55°/−3.90° and 36.85°/37.15°. The relocation was assessed by a double-difference earthquake location algorithm, which enhances the relative location of events, using the HypoDD code (Waldhauser, 2001; Waldhauser & Ellsworth, 2000). The P and S phase data recorded by the Spanish *Instituto Geográfico Nacional* (IGN) (National Geographic Institute, 2023),

10.1029/2023TC007956

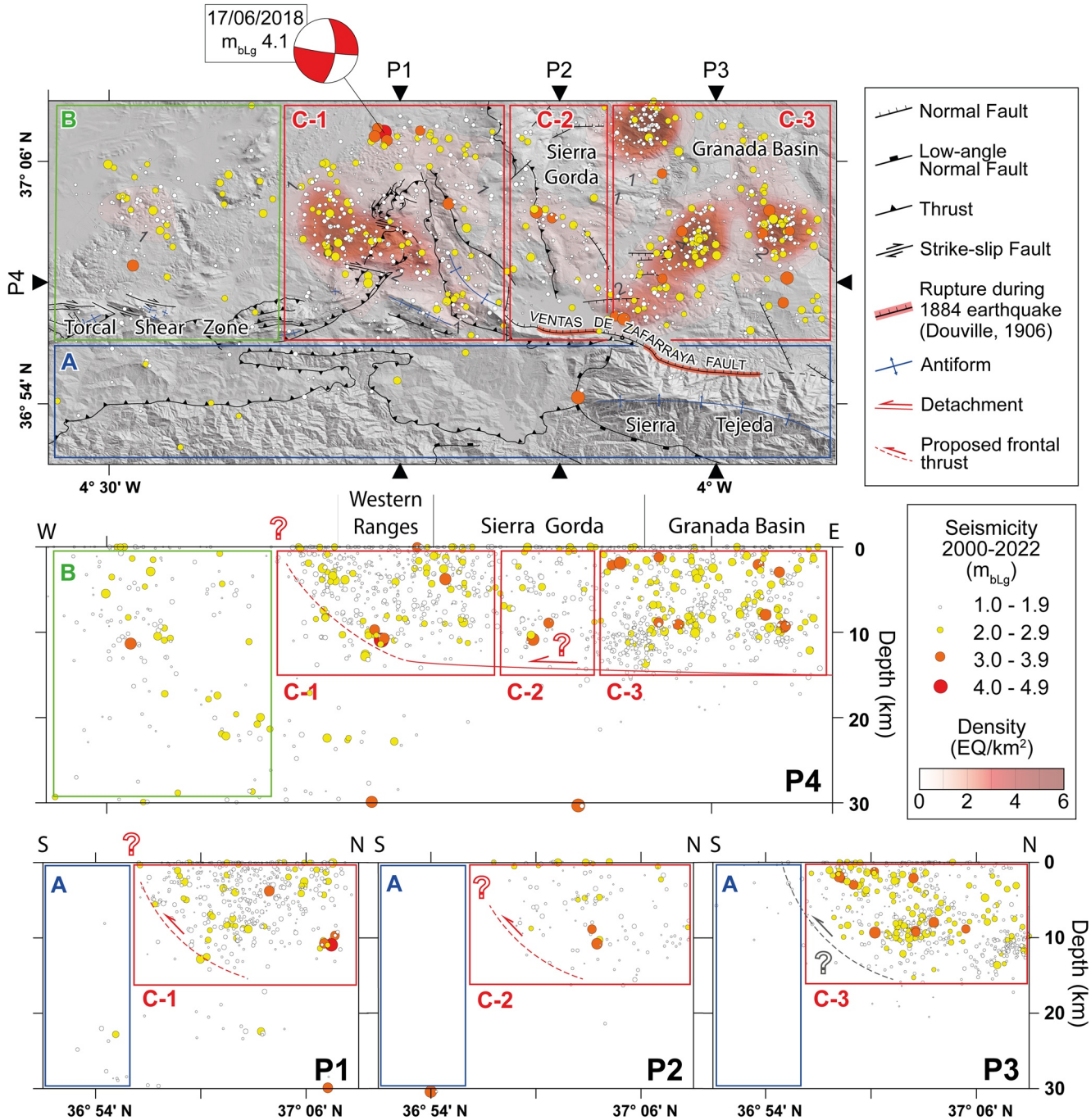

Figure 3. Map of the relocated seismicity (Table S1), including the projected seismicity on a W–E profile and three N–S cross-sections. The zones described in the results section are depicted in blue (a), green (b), and red (c). The maps show the earthquake focal mechanism associated with the highest magnitude event since the year 2000. The P4 profile includes all the relocated seismicity data. The P1, P2, and P3 profiles illustrate the seismicity in C-1, C-2, and C-3 red boxes, respectively, and their southern continuation.

derived from the permanent seismic network, as well as the velocity model of Palomeras et al. (2014), were used for the process (Figure 3; Table S1). All the available EFMs since 1985 were considered (Figure 4a; Table S2) to calculate the reduced stress tensors, using the Win-Tensor code and the inversion method developed by Delvaux and Sperner (2003) and Delvaux and Barth (2010). We calculated the stress tensor from mantle earthquakes and six crustal seismotectonic regions (Figure 4b; Table S3). Crustal seismotectonic regions are established based on the basis of both surface geological features and patterns of relocated seismicity. Regions with fewer than

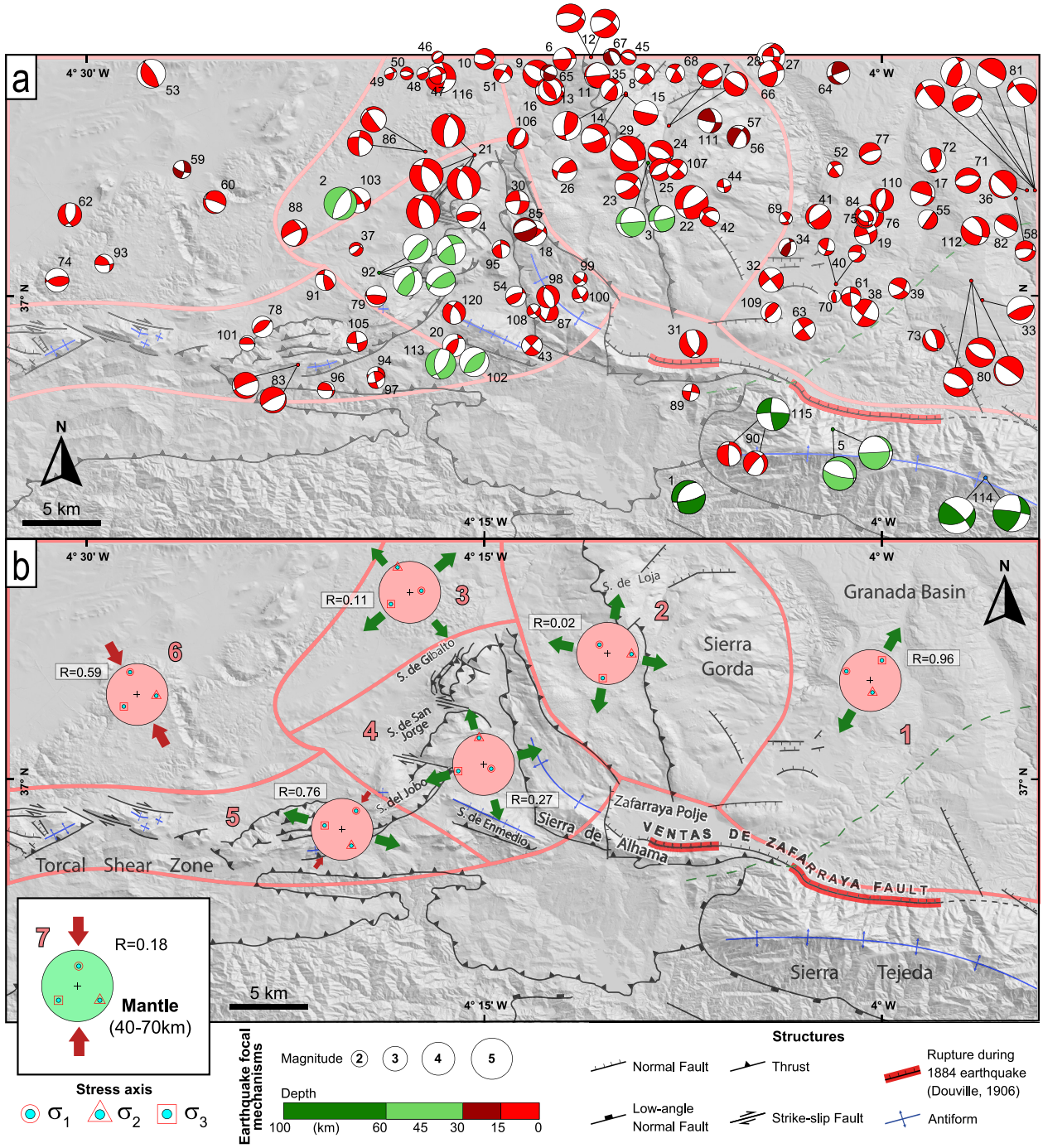

Figure 4. Earthquake focal mechanisms (EFMs) and reduced stress tensor. (a) EFMs used to compute the stress tensors, also shown in Table S2. Note that some earthquakes present different focal mechanism solutions. (b) Reduced stress tensor obtained for the 6 seismotectonic regions defined in the crust (delineated by light red lines) and mantle (number 7). R: indicates the axial ratio defined by $R = (\sigma_2 - \sigma_3)/(\sigma_1 - \sigma_3)$. The detailed results can be found in Table S3.

five recorded earthquakes have been excluded from consideration. Consequently, the Internal Zones of the Betic Cordillera and the Zafarraya Polje were excluded from this analysis. The western Granada Basin (1) coincides with an area of relatively high seismic activity. The Sierra Gorda massif (2) stands out due to its N–S striking thrust faults and its comparatively low seismicity. The Salinas (3) and Western Ranges (4) regions are associated with a zone of elevated seismic activity, which extends farther westward from the NE–SW and NW–SE striking mountain ranges that characterize the southern area (4). This region has been divided into two zones due to

10.1029/2023TC007956

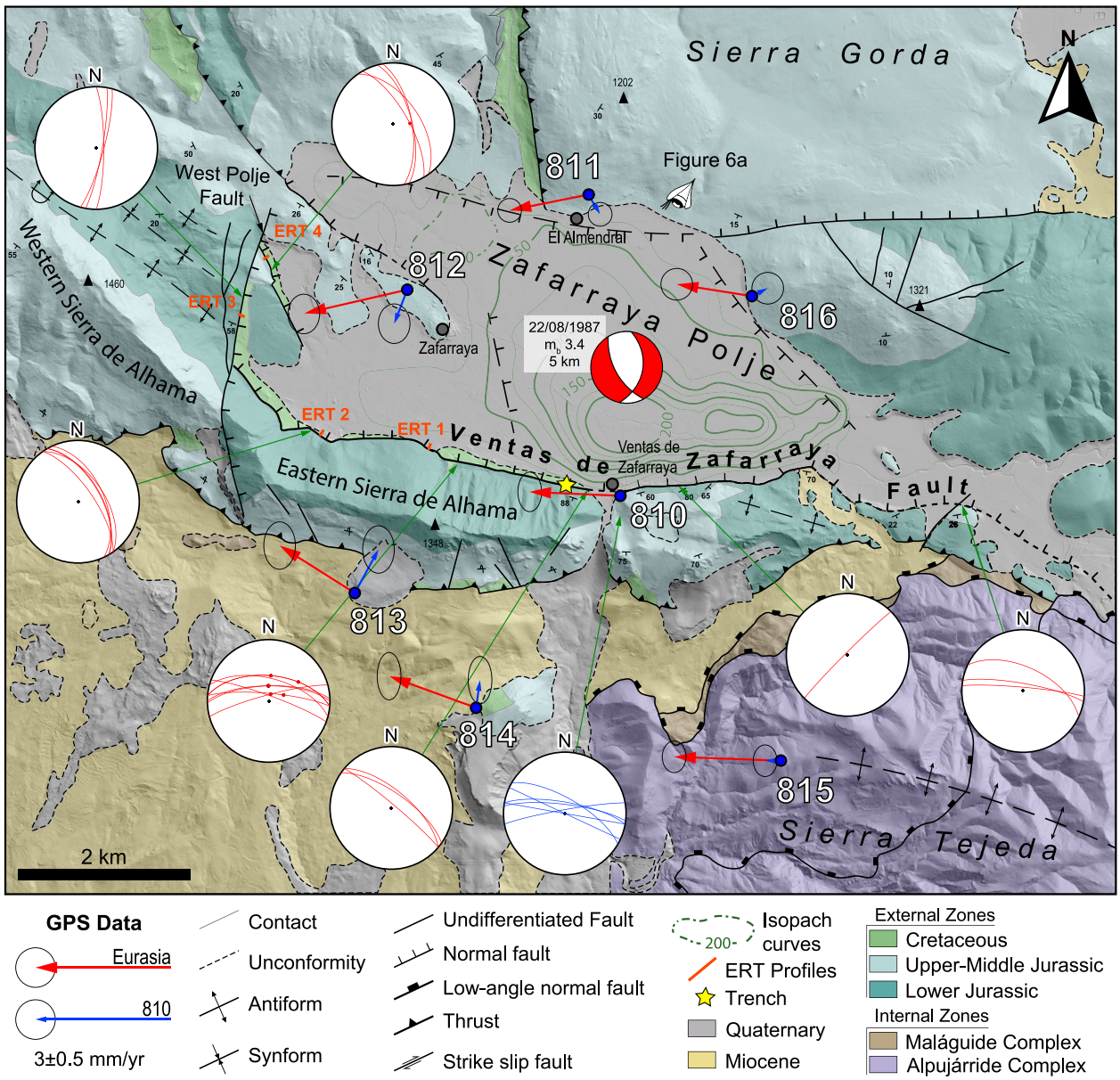

Figure 5. Geologic map of the Zafarraya Polje and Sierra de Alhama modified from Elorza et al. (1978) and Sanz de Galdeano (2013) including velocity vectors of the Zafarraya survey mode Global Navigation Satellite System network (Table 1). In red, with respect to fixed Eurasia. In blue, with respect to the fixed site 810. Stereonets (Smith lower hemisphere) of the faults (red) and joints (blue). Isopach curves are taken from García-Jerez et al. (2006).

different geological features and to ensure that the Iznajar 1998 seismic series, located in the northernmost region (3) and marked by strike-slip faulting (Carmona et al., 2009), does not exert any influence on the southern region (4). The Torcal Shear Zone (5) constitutes a transpressional region that has undergone relatively low seismic activity. Finally, the northwesternmost region (6) is affected by less deformation.

The GNSS data were acquired from a survey mode network installed in 2004 around the Zafarraya Polje (Gil et al., 2005) in order to quantify the current deformation related to the VZF (Figure 5). Sites 811, 812, and 816 are located in the hanging wall block of the fault, over limestones of the External Zones. In contrast, sites 810, 813, 814, and 815 are located in the footwall block. Both 810 and 813 lie over dolostone and limestone of the External Zones, and sites 814 and 815 over marbles of the Internal Zones. Every GNSS site consists of a concrete pillar anchored to solid rock with a forced centering device on top. The first survey was carried out in 2004 (Borque et al., 2005), the second in 2010 (Ruano et al., 2011), and subsequently in 2012, 2013, 2014, 2015,

Table 1
East and North Absolute Velocities, Uncertainties, and Residual Velocities (mm·yr^{-1}) With Respect to the Eurasia Fixed Reference Frame and With Respect to a Stable 810 Site

	Coordinates		Velocity		Uncertainty		Residual velocity (Iberia)		Residual velocity (site 810)	
Sites	Long. (°E)	Lat. (°N)	East	North	East	North	East	North	East	North
810	−4.120	36.956	17.6	16.6	±0.3	±0.5	−2.3	0.1	fixed	
811	−4.125	36.987	18.0	16.1	±0.3	±0.3	−2.0	−0.4	0.3	−0.5
812	−4.148	36.977	17.3	15.9	±0.4	±0.5	−2.6	−0.6	−0.3	−0.7
813	−4.155	36.946	18.0	17.7	±0.4	±0.6	−1.9	1.2	0.4	1.1
814	−4.139	36.934	17.7	17.3	±0.3	±0.6	−2.2	0.8	0.1	0.7
815	−4.099	36.929	17.3	16.7	±0.3	±0.4	−2.7	0.1	−0.4	0.0
816	−4.104	36.977	18.0	16.9	±0.4	±0.4	−1.9	0.3	0.4	0.2

and 2018 (Figure S1). During the 2004 and 2010 campaigns, seven Leica Geosystem GX1230 receivers and LEIAX1202 antennas were used for measuring.ing During subsequent campaigns in 2012, 2013, 2014, 2015, and 2018, seven Leica Geosystem AR10 receivers and LEIAR10 antennas were employed. In each campaign, all sites were observed continuously over four to five days, achieving a GNSS data record of 72 hr in 2010, 2012, and 2013 and 96 hr in 2014, 2015, and 2018 (Figure S1). All data were processed with the GipsyX software (Jet Propulsion Laboratory; Bertiger et al., 2020) using the PPP method. Position time series in the North and East components and absolute velocities were computed in the IGS14 reference frame. Finally, two residual velocity fields were estimated with respect to a fixed Eurasia frame and site 810 (Table 1).

Fieldwork was conducted to complement previous data (Figures 5 and 6). To elucidate the structural characteristics of the Sierra Alhama fold, we conducted bedding measurements in the basement of the External Zones. Detailed observations were made on scarps and surfaces of the Ventas de Zafarraya Fault –encompassing their orientation, dip, grooves, and striae orientations (Figures 6c and 6d)– to assess recent activity and fault kinematics. In addition, measurements of joints were made near the town of Ventas de Zafarraya (Figure 5). These surface data are complemented by previous geological observations (Elorza et al., 1978; Reicherter et al., 2003; Sanz de Galdeano, 2013) and geophysical prospecting data to provide insights into the shallow and deep structure of Zafarraya Polje and its surroundings (García-Jerez et al., 2006; Fernández-García & Ruano, 2016; Ollero Robles & García García, 1984.

To determine the shallow features and recent activity of the fault system, four ERT profiles were also deployed to measure resistivity and induced polarization (Figure 7). ERT images subsurface structures by measuring electrical resistivity, which helps to ERT maps subsurface structures with resistivity contrasts by measuring electrical resistivity, which helps to identify lithological changes associated with faults or the presence of fluids within fault zones. Induced polarization reveals faults when clays are present (Šumi, 1965) or metallic conductive mineral concentrations occur (Bleil, 1953). The induced polarization anomalies calculated along the ERT profiles are only significant in ERT-2; therefore, Figure 7 shows only this result. The southern ones (ERT-1 and ERT-2), are located over the VZF, whereas ERT-3 extends perpendicular to the N–S striking West Polje Fault in the western boundary of the basin. In turn, ERT-4 crosses a NW–SE striking fault. The profiles were acquired through the ABEM Terrameter SAS 4000 system using a 4-channel multiple gradient electrode array and applying GRAD4LX8 and GRAD4S8 protocols (ABEM, 2006) with 1 m electrode spacing. Inversion relied on the standard least squares model for constraining inversion with the Res2Dinv code (v 3.64, Geotomo Inc.; Loke, 2019).

3. Results

3.1. Relocation of Seismicity

The relocated seismic data of the study area since 2000 reveal seismicity reaching only magnitude m_{bLg} 4.1 (Table S1). Three zones were distinguished (Figure 3). On the one hand, the entire southern band (A-Blue) — corresponding to the Internal Zones— shows hardly any crustal seismicity. On the other hand, the northwestern zone (B-Green) shows some seismicity reaching depths of 20–30 km eastward. The north-northeastern zone

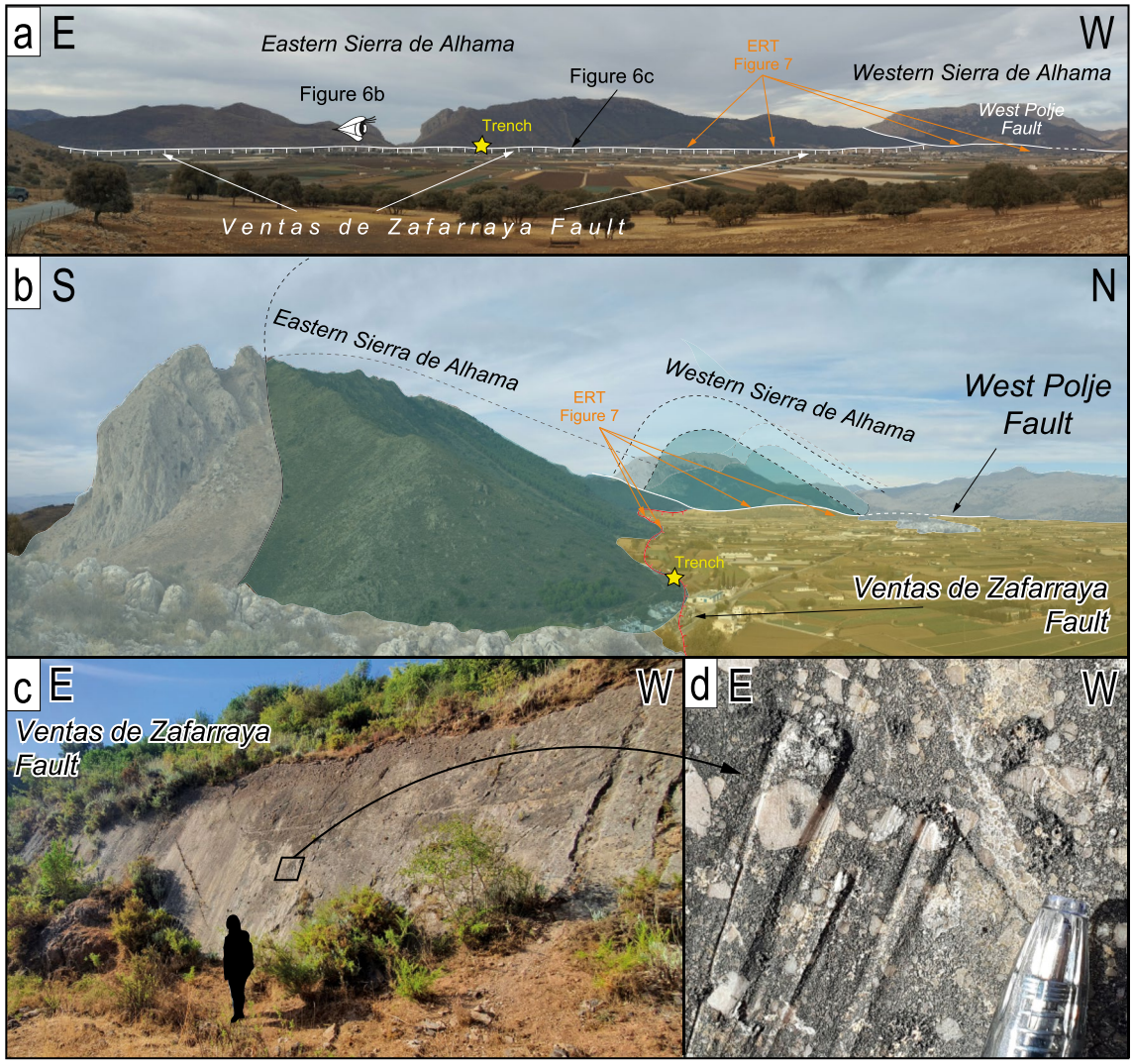

Figure 6. Main geological features of the Sierra de Alhama-Zafarraya Polje area. (a) Sierra de Alhama and a VZF panoramic view. (b) Interpretation of the Sierra de Alhama antiform over a field image. (c) Photo of the VZF plane. (d) Detail of normal to normal-dextral striae on the VZF plane.

(C-Red), with widespread seismicity limited to the first 10–15 km depth, can be subdivided into three sectors. West of Sierra Gorda (C-1) the seismicity draws an "*iron*" shape pointing westward. The seismicity is mainly limited to the first 10 km of the crust, but there are two small clusters at depths of 20 and 30 km. In this sector, the seismicity is more frequent to the west-southwest, following a NW–SE to WNW–ESE striking pattern, in continuity with the VZF. However, the highest magnitudes occur at the northern boundary (EFM in Figure 3). In the central sector (C-2), including Sierra Gorda and the Zafarraya Polje, seismicity decreases drastically. The eastern sector (C-3), located in the southwestern Granada Basin, has the highest number of earthquakes, with larger magnitudes than in the west, and the maximum depth increases up to 15 km.

3.2. Earthquake Focal Mechanism Solutions and Stress Tensors

The EFMs found in this region show great diversity (Figure 4a; Table S2). Although most of the EFMs are related to strike-slip faulting, some of them are also related to normal (Granada Basin) or reverse (SW of Sierra Gorda) faulting. The stress tensors computed from these solutions (Figure 4b; Table S3) indicate a 45° north-dipping N–S compression in the mantle (stress tensor 7; depth >30 km), while extensional stress tensors dominate in the upper crust (<20 km). The stresses are not uniform, however, we define six seismotectonic areas (Figure 4b). To the east, in the southwestern Granada Basin, stress tensor 1 shows a predominant NE–SW extension. To the

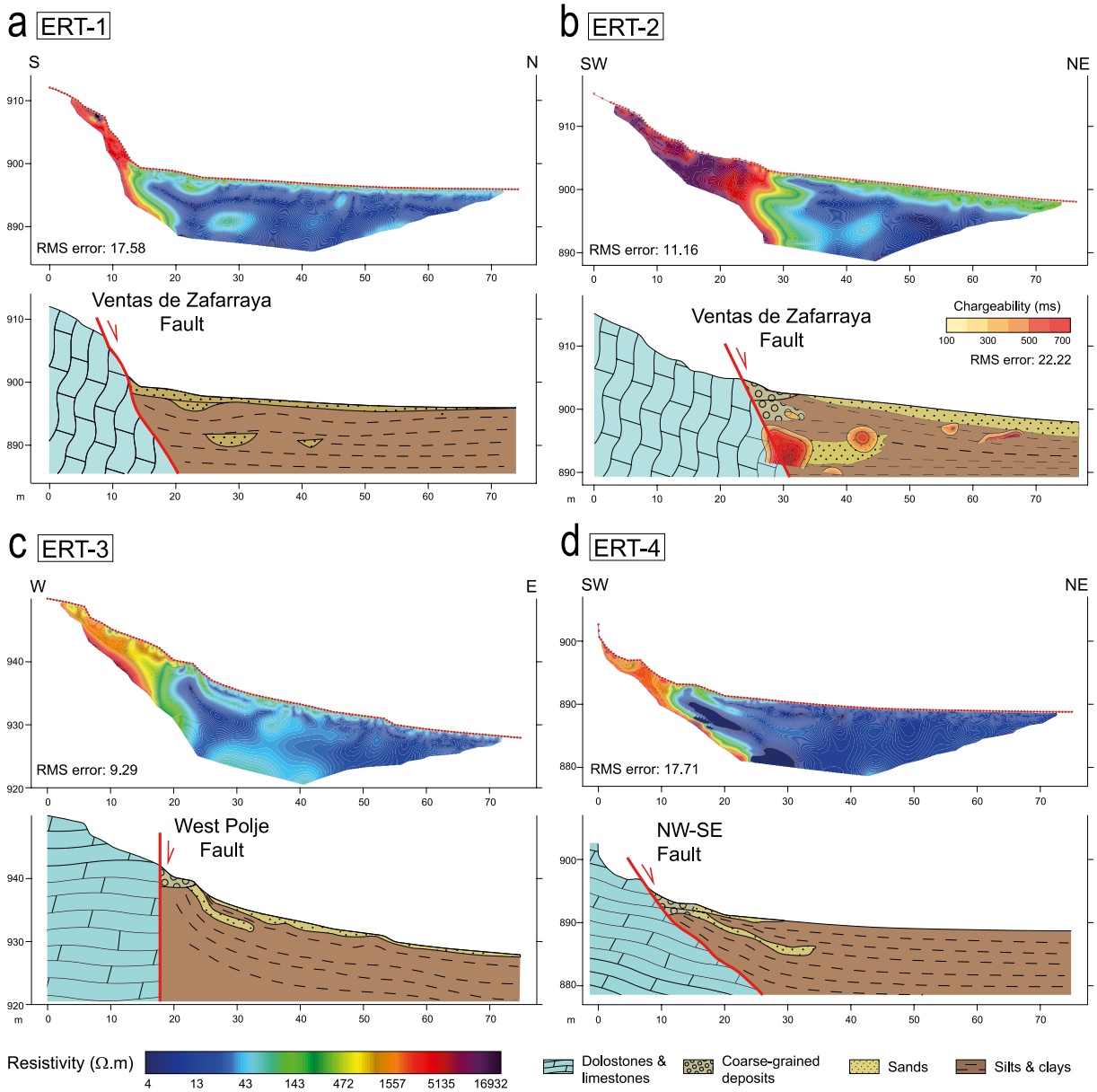

Figure 7. Electrical-resistivity tomography (ERT) profiles acquired in the Zafarraya Polje and their interpretations. (a) ERT profile acquired in an E–W striking segment of the VZF. (b) ERT profile acquired in a WNW–ESE striking segment of the VZF. The induced polarization is also shown for this profile. (c) ERT profile acquired in the N–S striking West Polje Fault. (d) ERT profile acquired in a NW–SE striking fault.

west, in Sierra Gorda and the western ranges, stress tensors (2, 3, & 4) show a nearly vertical σ_1 and an associated radial extension, especially in Sierra Gorda. Further to the west, the Torcal Shear Zone is characterized by a WNW–ESE extension (stress tensor 5). Finally, the NW section of the study area (stress tensor 6) is dominated by a NNW–SSE compressional stress regime.

3.3. Velocity Field of the Zafarraya Survey Mode GNSS Network

Considering a fixed Eurasian frame (red arrows in Figure 5), all the velocity vectors of the Zafarraya survey mode GNSS network roughly point to the west, with mean rates between 1.9 and 2.7 mm/yr (Table 1). Sites 810 (2.3 mm/yr) and 815 (2.7 mm/yr) point to the W, sites 813 (2.3 mm/yr), 814 (2.3 mm/yr), and 816 (1.9 mm/yr) to the WNW, and sites 811 (2.0 mm/yr) and 812 (2.7 mm/yr) to the WSW. Considering site 810 as a fixed point allowed us to evaluate the local deformation of the Zafarraya Polje and the VZF (blue arrows in Figure 5). Sites

813 (1.2 mm/yr) and 814 (0.7 mm/yr) point to the NNE, 812 (0.8 mm/yr) to the SW, 811 (0.6 mm/yr) to the SE, and 816 and 815 show negligible motion. A ∼2 mm/yr NNE–SSW shortening is calculated between sites 812 and 813, a ∼1 mm/yr shortening with some dextral component between 811 and 814, and no shortening is observed between 815 and 816.

3.4. Structure of the Sierra de Alhama and the Zafarraya Polje

The Zafarraya Polje is a W–E elongated Quaternary basin located in the External Zones, near the Internal/External Zones boundary (Figure 2). It is surrounded by several mountain ranges. To the north, the Subbetic rocks of Sierra Gorda are mainly affected by N–S to NW–SE striking and eastward-dipping thrusts. To the SW, these structures bend and strike WNW–ESE (Elorza et al., 1978), forming Sierra de Alhama. The Sierra de Alhama range (Figures 2 and 5) is an antiform with two well-defined sectors. The western part, located to the west of the Zafarraya Polje, strikes from WNW–ESE to W–E. The eastern part is partly collapsed and forms the Zafarraya Polje, making the fold axis difficult to trace (Sanz de Galdeano, 2013). The fold is formed by a subvertical forelimb mainly dipping to the south, in some places with overturned bedding that limits the Zafarraya Polje from the south (Figure 6b). The backlimb, sometimes collapsed, dips to the north, ranging from 50° to 10°. To the east, near the Internal/External Zones boundary, it disappears (Figure 4). The Sierra Tejeda antiform is the main structure found southeast of the Zafarraya Polje. It strikes ESE-WNW to E–W and affects the Alpujárride Complex (Fernández Fernández et al., 1992).

Ambient noise, gravity, and vertical electrical sounding surveys were used to determine the Zafarraya Basin architecture (Fernández-García & Ruano, 2016; García-Jerez et al., 2006; Ollero Robles & García García, 1984). They indicate a main depocenter reaching a depth of 200 m in the eastern half of the Zafarraya Polje. The western half is not as deep as the eastern half, reaching a few tens of meters by the southern and northern boundaries, while the basement crops out in the middle (Figure 5).

The E–W striking VZF is the main recent structure in the region (Figures 5 and 6a), having normal to normal-dextral striae (Figure 5, stereonets; Figure 6d) (Reicherter et al., 2003; Ruano et al., 2004; Sanz de Galdeano, 2013). Different segments can be observed. To the W, in the Zafarraya Polje (Figures 2 and 5), it strikes WNW–ESE to W–E, and an escarpment of up to 1.5 m is preserved. The VZF is more difficult to detect in the field across the Internal/External Zones boundary and it does not have such a pronounced geomorphologic imprint. Toward the east (Figure 2), it strikes W–E accompanied by a marked geomorphologic discontinuity in the northern flank of the Sierra Tejeda antiform (Alonso-Chaves & Orozco, 2007; Reicherter et al., 2003). The West Polje Fault is another major fault, limiting both the Zafarraya Polje and the VZF to the W, striking N–S, and dipping sharply to the E (Figures 5 and 6). There are further W–E, N–S, and NW–SE striking minor faults in the basin, both observable in the field and interpreted from geophysical data (Fernández-García & Ruano, 2016; Sanz de Galdeano, 2013).

3.5. Electrical-Resistivity Tomography

The ERT-1 and ERT-2 profiles, located over the VZF (Figures 7a and 7b), show a high resistivity block in the southern part with respect to a northern conductive block. The discontinuity between them is an approximately 60° north-dipping surface, indicative of a fault that divides the dolostones of the footwall block and the Quaternary detrital sediments of the hanging wall block. The wedge-like high resistivity anomalies located on the fault plane in ERT-2 suggest the presence of coarse-grained wedge-like deposits in the hanging wall of the fault (Figure 7b). Induced polarization was also measured in the ERT-2 profile. The highest chargeability values occur at 30 m from the beginning of the profile and at an elevation of 894 m, coinciding with the resistivity discontinuity, supporting the existence of a fault. ERT-3 (Figure 7c) shows that the N–S striking West Polje Fault has an almost vertical dip separating a resistive block formed by limestones from a conductive block formed by recent sediments. Coarse-grained levels can be interpreted in the eastern subsided block, forming a drag-fold. Finally, ERT-4 images a nearly 45° normal fault dipping to the NE that separates the resistive limestones from the recent sediments (Figure 7d).

4. Discussion

4.1. Bending-Moment Fault Activity: The Ventas de Zafarraya Fault

The development of fold-related fractures is a well-known phenomenon (Li et al., 2018; Yeats et al., 1981). However, such structures are considered secondary in the region (Stephenson et al., 2007). New studies have

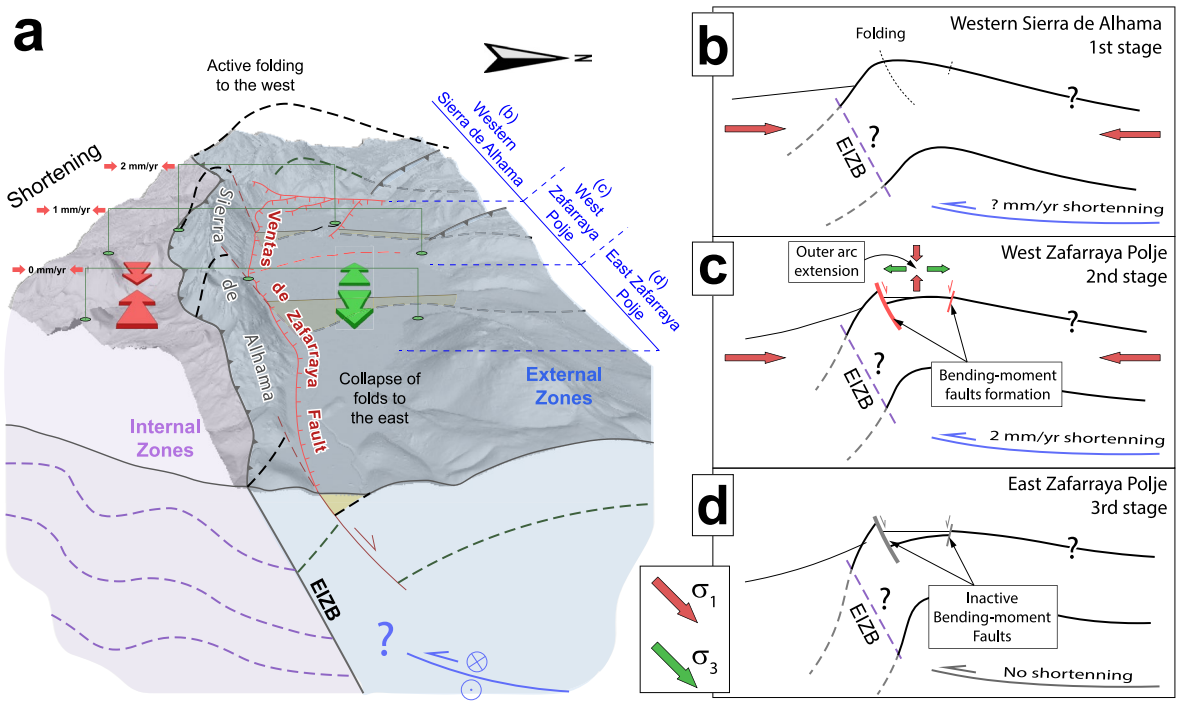

Figure 8. Proposed 3D model of the Sierra de Alhama-Zafarraya Polje area. (a) Zones distinguished in the Sierra de Alhama-Zafarraya Polje area. (b–(c) N–S cross sections crossing Sierra de Alhama and Zafarraya polje. EIZB: External/Internal Zones Boundary. (b) first stage. Initial development of the Sierra de Alhama antiform: western Sierra de Alhama. (c) second stage. Development of the Sierra de Alhama antiform and activity of the Ventas de Zafarraya bending-moment fault: west Zafarraya Polje. (d) third stage. Inactive Sierra de Alhama antiform and Ventas de Zafarraya Fault: east Zafarraya Polje.

analyzed the recent activity of these structures using geological techniques (Li et al., 2018), but a detailed quantification of the ongoing surface deformations (Gil et al., 2017) generating them has not been achieved. The data from the Zafarraya near-field GNSS network (Gil et al., 2005) presented here (Figure 5) provide an opportunity to quantify the deformation along an active normal fault (Reicherter et al., 2003) developed within the core of a parallel fold formed by a perpendicular contraction.

The VZF is the main active extensional structure to the southwest of the Granada Basin, as evidenced by the associated WNW–ESE striking large scarps and striae indicating normal to normal-dextral slip and NNE–SSW extension (Ruano et al., 2004; Sanz de Galdeano, 2013). Together with the main fault, N–S striking and eastward-dipping normal faults and NW–SE striking and NEward-dipping normal faults occur in the Zafarraya Polje (Elorza et al., 1978; Sanz de Galdeano, 2013) (Figure 5). Furthermore, geophysical data (Fernández-García & Ruano, 2016; García-Jerez et al., 2006; Ollero Robles & García García, 1984) and an EFM suggests NNW–SSE and N–S striking buried faulting in the central part of the polje (Figure 5). Most of these faults cut the most recent sediments (Figure 7). Moreover, coarse-grained wedge-like deposits crop out in the field, in a trench located 3 km to the west (Figures 5 and 6) (Grützner et al., 2013; Reicherter et al., 2003). Three coarse-grained wedge-like deposits were interpreted as colluvial wedges, features usually indicative of coseismic ruptures (McCalpin, 1996). C14 dating of soils between three colluvial wedges, the two deepest of which are affected by recent faults, indeed indicates at least three events in the last 9,000 years. The shallowest colluvial wedge is not affected by faulting and is correlated with the 1884 Andalusian earthquake (Reicherter et al., 2003). Therefore, the coarse-grained wedge-like deposits interpreted in ERT-2 could be due to the presence of one or more of these colluvial wedges, supporting Holocene activity also in the western sector. All these data suggest very recent normal fault activity consistent with N–S to NNE–SSW extension. However, GNSS data determine that an active NNE–SSW shortening and a small E–W lengthening affect the area. In addition, the fact that the Zafarraya Polje has hardly any seismicity would suggest an apparently contradictory setting.

The shortening calculated in the GNSS network points to the current development of the WNW–ESE to W–E striking Sierra de Alhama antiform (Figure 8a). The activity of the VZF and other minor normal faults may therefore be related to folding, in agreement with Galindo-Zaldívar et al. (2003) and Ruano et al. (2004). Bending-moment faulting of a fold can generate parallel, transverse, and oblique normal faults (Stephenson et al., 2007). Typically,

transverse and oblique faults predominate, which could accommodate maximum strain perpendicular to compression, as occurred in the Sirian Arc (Moustafa, 2013). In the Zafarraya Polje, NW–SE striking oblique and N–S striking transverse faults may accommodate the E–W extension observed by the GNSS network in the northern part, further supported by an EFM (Figure 5). In any case, the main VZF is perpendicular to the shortening and subparallel to the fold axis, like other smaller faults interpreted in the basin (Fernández-García & Ruano, 2016; Sanz de Galdeano., 2013). This fold-parallel faulting appears to be influenced by the geometry of the fold. As shown in the study conducted by Li et al. (2018), a reduction in the interlimb angle tends to decrease the width of the fault zone and concentrate the most prominent fault scarps in a narrow zone. The extension of the outer arc of the fold is influenced by its proximity to the neutral surface and bed curvature (Ramsay, 1967; Tavani et al., 2015). As the interlimb angle decreases the distance to the neutral surface may reduce and the bed curvature increases. The combination of these factors leads to promoting extension and faulting concentration within a narrow, highly deformed zone (Li et al., 2018). According to these authors folds with an interlimb angle below 100–120° tend to concentrate at least 30% of the cumulative fault scarp height along the fold within a single fault or in a very narrow zone, as observed in the Atushi or Hermodun folds. The Sierra de Alhama antiform exhibits an interlimb angle ranging between 50° and 100°. By the examples mentioned earlier, the VZF has a significant scarp compared to other faults within the Polje de Zafarraya (Figures 5 and 8a). In addition, the more asymmetric the fold, the more faulting toward the backlimb (Li et al., 2018). Thus, the subvertical forelimb of the Sierra de Alhama antiform with respect to a 10º–50° backlimb would explain why the faulting appears to the north of the hinge (Figures 5 and 6). The above considerations support the activity of the VZF as a bending-moment fault, as occurs in other cases including Zagros Mountains, Iran (Stephenson et al., 2007), Pamir-western Kunlun and southern Tian Shan regions, northwestern China (Li et al., 2018) and El Asnam, Algeria (Meghraoui & Doumaz, 1996).

Shortening and fault slip are not uniform along the entire axis of the fold. Three sectors can be distinguished in the Sierra de Alhama-Zafarraya Polje (Figures 5 and 8a). (a) The eastern part of the Zafarraya Polje is characterized by the deepest depocenter, reaching 200 m (García-Jeréz et al., 2006). The western limit of the depocenter is a N–S to NNE–SSW striking discontinuity not affecting the VZF, probably associated with a buried high-angle normal fault that dips to the east (Sanz de Galdeano., 2013) supported by an EFM (Figure 5). (b) The basement in the western half of the Zafarraya Polje is shallow and crops out in some places, indicating a shallower position of the basement with respect to the eastern half. The western boundary is the subvertical N–S striking West Polje Fault (Figure 7c). (c) The western Sierra de Alhama constitutes an antiform without major fractures (Figure 5; Elorza et al., 1978). These data suggest that the Sierra de Alhama antiform collapsed eastwards forming the Zafarraya Polje. GNSS data show that the eastern part of the Zafarraya Polje shows negligible shortening indicating no ongoing collapse, whereas the western part is affected by a nearly 2 mm/yr NNE–SSW shortening with related active collapse. The seismicity (Figure 3) also indicates that the current tectonic activity is shifting to the west. The westward continuation of the Sierra de Alhama-Zafarraya Polje area is affected by low and low-to-moderate seismicity (Figure 3). These data suggest a westward migration of the shortening and folding in the Sierra de Alhama-Zafarraya Polje (Figure 8a). The eastern Zafarraya Polje is currently inactive, and bending moment faulting of the VZF collapsed the fold (Figure 8d). The Zafarraya Polje has undergone less collapse in the west, though fold development appears to be active due to convergence observed in the GNSS data. Additionally, there are many active bending-moment faults. Seismicity suggests that the western Sierra de Alhama may currently be under compression, with an incipient fault development. However, we cannot rule out the possibility that other factors, such as lower shortening rates or fold geometry, that may be responsible for the lack of faulting in this western sector.

The new GNSS data confirm that active normal faults can develop in the context of perpendicular contraction. Moreover, the activity of the faults would be determined by the folding associated with the shortening, as proposed by the so-called bending-moment faults (Li et al., 2018; Livio et al., 2019; Yeats et al., 1981). Furthermore, it highlights the importance of these faults, which can extend for tens of kilometers acting as regional sources of seismic activity (Reicherter et al., 2003; Sanz de Galdeano et al., 2003).

4.2. Active Compressional Front in an Extensional System: W and SW Granada Basin

The data presented in this study contribute to a better characterization of the W and SW boundaries of the Granada Basin and place the tectonic activity of the Sierra de Alhama-Zafarraya Polje area within a regional context.

While the Granada Basin is characterized by extensional structures (Galindo-Zaldívar et al., 2015; Madarieta-Txurruka et al., 2021; Martín-Rojas et al., 2023), the tectonic activity to the west is more heterogeneous (Figure 2). From south to north, the activity changes as follows: (a) in the Internal Zones, to the south, there is no significant crustal seismicity, although the current development of Sierra Tejeda (Ruano et al., 2004) suggests NE–SW compression, (b) the central sector (Figure 5) is characterized by a NNE–SSW shortening observed by the Zafarraya GNSS network, and (c) the western sector, around Sierra Gorda, is more complicated (Figure 2), being affected by recurrent seismicity limited to the north by a dextral discontinuity (EFM in Figure 3) (Iznájar 1998 sequence; Stich et al., 2003). While Quaternary compressional structures appear in the NW Granada Basin (Ruano et al., 2004), the Sierra Gorda and western ranges are characterized by radial extension. Further west, however, stress tensors #1 and #5 indicate NW–SE and NE–SW compression, respectively suggesting a transition from extension in the east to compression in the west between seismotectonic regions #1 and #5 and regions #2 and #6 (Figure 4). This location coincides with the western limit of the iron-shaped upper-crustal seismicity indicating a deformation front (Figure 3). Therefore, we propose an arcuate front of compressional deformation starting west of Sierra Gorda, traversing the Sierra Alhama-Zafarraya Polje area with a WNW–ESE orientation, then striking NW–SE and E–W in the Sierra Tejeda antiform (Figure 9a). At depth, the seismicity exhibits an east-dipping discontinuity that reaches about 10 km in the western boundary (C-1 red box in Figure 3). In the western Granada Basin (C-3 red box in Figure 3) the seismicity reaches a depth of 15 km, matching that of the central and eastern Granada Basin (Galindo-Zaldívar et al., 1996, 1999; Madarieta-Txurruka et al., 2021). These data point to a current kinematic relationship between the compressional front and the extensional detachment of Granada. Galindo-Zaldívar et al. (2000) previously proposed this connection for the Miocene evolution.

The observations presented in this paper are consistent with continuous GNSS data (Galindo-Zaldívar et al., 2015) (Figure 9 and Figure sS2). On the one hand, LOJA and PALM sites record a lengthening with respect to the fixed NEVA site in Sierra Nevada, the highest part of the mountain range. The motion rotates from NE–SW in the south to E–W in the north. This would support an E–W to NE–SW radial extension in the Granada Basin with respect to Sierra Nevada (Figure 9b). On the other hand, if we compare the velocity rates of LOJA and PALM with respect to MALA (Figure 9c), a shortening of the E–W component of the displacements can be observed. At the same time, a shortening of the N–S component of PALM compared to MALA is also registered. In contrast, an N–S extension is observed for LOJA. These data support the existence of a compressional to sinistral deformation zone between these sites. NE–SW compression occurs between PALM and MALA, while sinistral motion is registered between LOJA and MALA. This front is also consistent with the data published by Martín-Rojas et al. (2023), suggesting a compression of up to 0.6 mm/yr.

All these data point to a general model of a top-to-the-W-SW gravitational collapse over the detachment of the extensional system of the Granada Basin (Galindo-Zaldívar et al., 1996; Madarieta-Txurruka et al., 2021, 2023b; Ruano et al., 2004). In this regional setting, the W and SW of Granada Basin may conform to a nearly fixed boundary (Rey et al., 2001) that slows down the W–SW displacement and produces local compression (Figure 9a), as in the Main Central Thrust and the South Tibetan Detachment System (Burchfiel & Royden, 1985). This boundary could be related to a high Bouguer gravity anomaly located in Málaga (Figure 1b), associated with high-density ultramafic rocks embedded in the crust of the Internal Zones (Pedrera et al., 2020; Torné et al., 1992). The fact that the boundaries of this body coincide with the trace of the compressional front would suggest it acts as a buttress (Woodward, 1988). Furthermore, together with the differences between the External and Internal Zones, this body could cause the heterogeneity of the front. The northern sector —located in the External Zones— is offset to the west and characterized by seismicity, indicative of a west-vergent thrusting. The southern sector, in the Internal Zones, lies east of the high-density body. This sector is affected by folding, as evidenced by the formation of the Sierra Tejeda antiform and the absence of seismicity.

As occurs in the Sierra de Alhama-Zafarraya Polje area, the proposed westward migration could extend at least to the northern sector of the study area (Figure 9d). The migration of the extensional system of the Granada Basin has been suggested before (Galindo-Zaldívar et al., 1996; Madarieta-Txurruka et al., 2021; Martinez-Martinez et al., 2002). Similarly, the new seismicity relocation (Figure 3; P4) indicates that a new thrust front is developing to the west of Sierra Gorda. This new thrust will eventually take form beneath the Miocene ones (Galindo-Zaldívar et al., 2000), uplifting them and inducing radial extension associated with gravitational instability in Sierra Gorda (Figures 4 and 9d) in a piggyback sequence.

The connection between extensional detachments and fold and thrust fronts has been suggested in several orogens worldwide in relation to fixed-boundary gravitational collapse (e.g., Burchfiel & Royden, 1985; Foster et al., 2023; Rey et al., 2001). The example of the extensional system of the Granada Basin indicates that compressional

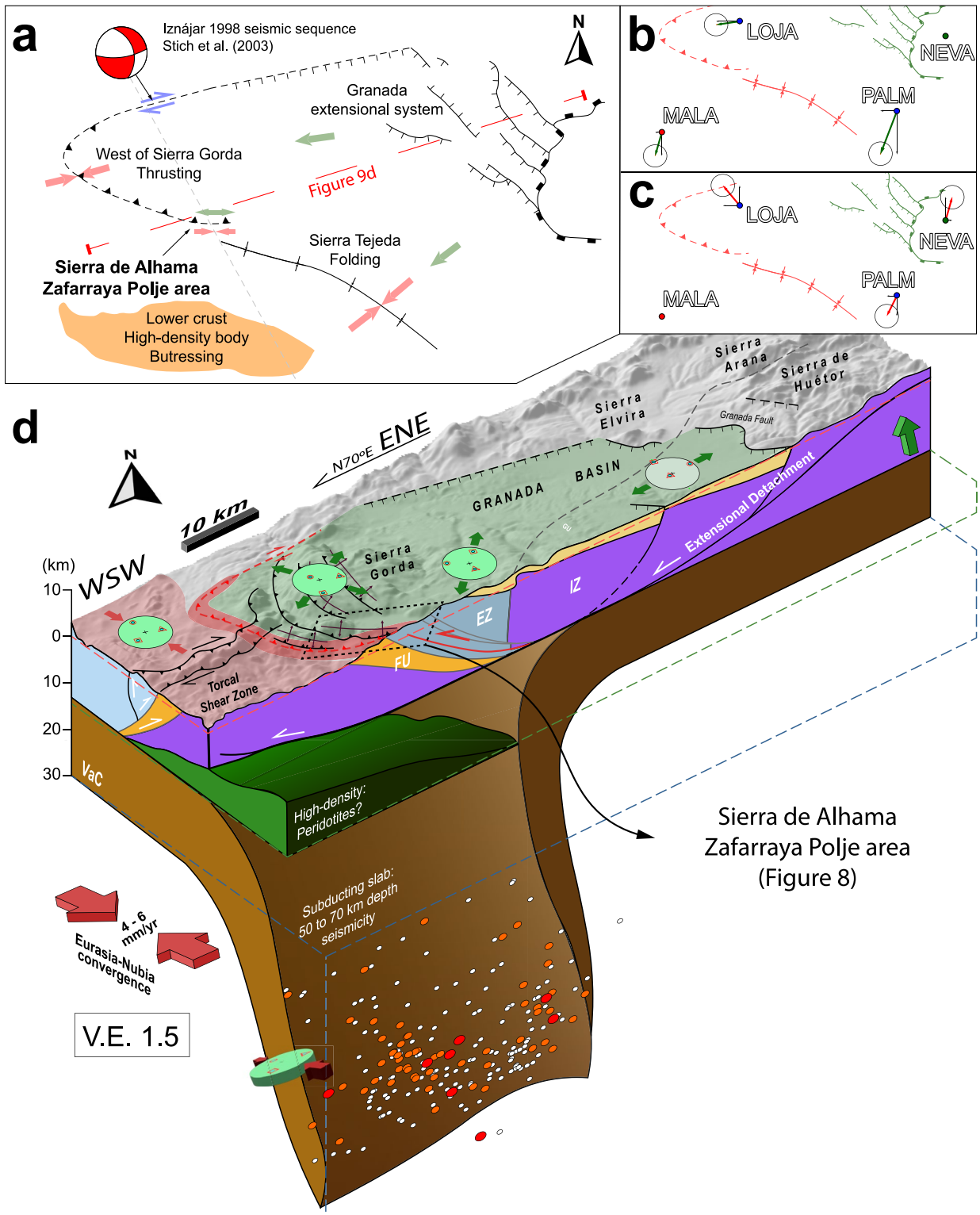

Figure 9. Tectonic model of the central Betic Cordillera. (a) Sketch of the westward-directed gravitational collapse model of the central Betic Cordillera. (b & (c) Global Navigation Satellite System data from Galindo-Zaldívar et al. (2015) and major structures. (b) Green arrows represent velocity rates relative to the fixed NEVA: LOJA and PALM show an almost radial extension. (c) Red arrows represent velocity rates with respect to fixed MALA: PALM shows NE–SW shortening. LOJA shows minor N–S lengthening and relative sinistral motion. (d) Proposed 3D model for the central Betic Cordillera. The green colored zone indicates an area affected by extension, the solid red indicates the proposed shortening front, and the light red marks regional compression. Stress tensors are projected and include those determined by Madarieta-Txurruka et al. (2021). Intermediate (50–70) seismicity from IGN (National Geographic Institute, 2023) is shown above the subducting slab. V.E.: Vertical Exaggeration. EZ: External Zones; IZ: Internal Zones; FU: Flysch Unit; VaC: Variscan Crust.

fronts can also form in nearly fixed-boundary collapses. The crustal heterogeneities under the detachments act as buttresses (e.g., Boyer, 1995; Mitra, 1997) and decrease the extension rate, generating localized shortening.

4.3. Implications for the Source of Destructive Earthquakes: The 1884 Andalusian Earthquake

The VZF is the main active fault near the epicenter of the 1884 Andalusian earthquake (Reicherter et al., 2003). According to the Quaternary-Active Faults Database of Iberia (QAFI, 2023), a 20 km long active fault is considered as the Ventas the Zafarraya Fault, capable to host Mw 6.5–6.6 earthquakes (Wells & Coppersmith, 1994). Udías and Muñoz (1979) point to a rupture area related to the Andalusian earthquake that is as long as the fault. However, Reicherter et al. (2003) describe two segments as the surface rupture (Douvillé, 1906), separated by a segment affected by NE–SW and NW–SE striking extensional cracks (López Arroyo et al., 1980). The model proposed here suggests that the VZF in the western segment may be active due to fold development in the Sierra de Alhama, while the central segment in the eastern Zafarraya Polje is currently inactive as no deformation is recorded (Figure 5). The 6 km long segment in the western Zafarraya Polje could host a Mw 5.9 earthquake, considering its surface length (Wells & Coppersmith, 1994), significantly lower than the Mw 6.5 estimated for the 1884 earthquake (Mezcua et al., 2004). The eastern segment, in the northern foothills of Sierra Tejeda, is a 10 km long segment that could host a Mw 6.2 earthquake. If both segments were activated simultaneously, the earthquake could reach Mw 6.4, like the estimated magnitude. Meanwhile, the 4 km long central segment, which is affected by extensional cracks, could be activated at depth without causing significant rupture at the surface. In this context, the 1884 Andalusian earthquake would been triggered by the activation of at least the bending-moment fault segment of the western Zafarraya Polje, the segment associated with the collapse of the northern limb of Sierra Tejeda (Reicherter et al., 2003; Ruano et al., 2004) and probably by the central segments connecting them at depth.

Even if surface ruptures are observed, deeper sources should be considered given the assigned hypocentral depth of 10–20 km (Udías & Muñoz, 1979). Fold-related faults can be activated by events in basal detachments, as occurred in the El Asnam thrust, Algeria (Meghraoui & Doumaz, 1996). The new data indicate that the extensional system of the Granada Basin is linked to the compressional front through a detachment reaching a depth of about 15 km in the area of the earthquake hypocenter. Both the Sierra de Alhama-Zafarraya Polje area and the Sierra Tejeda antiform are probably rooted there; their development would accordingly be controlled by this detachment. In this context, the main event could have occurred in the detachment and produced related events on the surface faults, generating the described rupture zones. In contrast, detachment can work by creep, without generating relevant earthquakes, until it destabilizes the surface area and activates the segments described above.

From the perspective of seismic hazard, bending-moment faults are structures that need to be carefully taken into consideration. New data suggest that these faults can constitute the main seismogenic faults of the region, which, temporally accompanied by other processes, such as gravitational collapse, can lead to moderate earthquakes with magnitudes reaching close to Mw 6.5, as seen in the 1884 Andalusian earthquake. Furthermore, slip on regional deep detachments, either during seismic events or due to creep, could facilitate the activity of these shallow normal faults (Meghraoui & Doumaz, 1996).

4.4. Geodynamic Implications

The extensional system within the Granada Basin, affecting mainly the upper crust (as shown in Figures 3, 4 and 9) (Galindo-Zaldívar et al., 2015; Madarieta-Txurruka et al., 2021), is integrated into the broader context of the Eurasian-Nubian convergence. The suggested compressional front of this system is located near the transition zone between the central and western Betic Cordillera. Deep geophysical data (Banda & Ansorge, 1980; Banda et al., 1993; Díaz et al., 2016; Galindo-Zaldívar et al., 1997), indicating crustal thickening of up to 40 km beneath the central Betic Cordillera, as well as the lack of intermediate-depth seismic activity in this area, suggest that subduction is not currently active in this area. Mancilla et al. (2015; among others) propose that slab-tearing processes detached the subducting slab and led to rapid uplift and exhumation of the shallowest portion of the slab located above the tearing, effectively doubling the crust (Platt et al., 2006). In contrast, the western Betic Cordillera is characterized by convergence (González-Castillo et al., 2015b; Ruiz-Constán et al., 2009). Intermediate-depth seismicity beneath the Malaga coast (Figure 9d) (Santos-Bueno et al., 2019) and seismic tomography (Blanco & Spakman, 1993) indicate an ongoing subduction process (Morales et al., 1999; Pedrera et al., 2011) involving

an E–W to NE–SW striking slab attached to the continental margin that dips southeastward. Furthermore, seismological data indicate that rollback may be occurring during subduction, and that the slab could be currently detaching westward beneath Málaga (e.g., Meighan et al., 2013; Ruiz-Constán et al., 2011), which is consistent with the mantle stress tensor #7 computed here (Figure 4). This tensor depicts an N–S trending σ1 (Table S3) with an inclination of 43ºN, implying a radial extension ($R = 0.18$) subparallel to the slab.

Uplift in the central Betic Cordillera related to the exhumation of the metamorphic complexes (Braga et al., 2003; Reinhardt et al., 2007), as seen in the Nevado-Filábride Complex, in the Internal Zone, would explain gravitational collapse into surrounding areas (Rey et al., 2001) along extensional detachments (Galindo-Zaldívar et al., 1996; Madarieta-Txurruka et al., 2021). However, the extension is not perpendicular to the mountain range (Rey et al., 2001) or even radial with respect to the most uplifted area, Sierra Nevada (Dewey, 1988). On the one hand, this could be due to the interaction of the NW–SE plate convergence and the active rollback, mainly registered in the western Betic Cordillera (González-Castillo et al., 2015a), which produces the highest rate of subsidence and thinning in the Western Alborán Basin (Do Couto et al., 2016; Torné et al., 2000), facilitating collapse toward the W–SW (Figures 1 and 9a). On the other hand, active Eurasia-Nubia compression (DeMets et al., 2010; McClusky et al., 2003; Nocquet & Calais, 2003) thickens the crust to over 30 km north of Sierra Nevada (Pedrera et al., 2020), preventing northward collapse. This would facilitate a lateral extrusion (Ratschbacher et al., 1991) to the west through a boundary formed by dextral strike-slip faults (Galindo-Zaldívar et al., 2015; Stich et al., 2003) north of Sierra Gorda and the Granada Basin (Figure 9a). Finally, the westward migration of the gravitational collapse system since the Miocene (proposed here) is consistent with both westward rollback of the Gibraltar Arc (e.g., González-Castillo et al., 2015a; Rosenbaum et al., 2002; Van Hinsbergen et al., 2014; Zeck & Whitehouse, 1999) and east-to-west slab tearing (e.g., Chertova et al., 2014; Garcia-Castellanos & Villaseñor, 2011; Mancilla et al., 2015).

Regions where plate convergence and subduction with rollback interact, such as Mediterranean orogenic arcs (e.g., Van Hinsbergen et al., 2014; Wortel & Spakman, 2000), the Banda Arc in eastern Indonesia (Pownall et al., 2013; Spakman & Hall, 2010), or the Scotia Arc between South America and Antarctica (Barker, 2001; Morales-Ocaña et al., 2023; van de Lagemaat et al., 2021), are conducive to the development of extensional detachment systems. The uplift of certain areas, attributed to crustal thickening resulting from thrust and fold development (Tricart et al., 1994), shear zones (Morales-Ocaña et al., 2023), and/or slab tearing (Delph et al., 2017; Parera-Portell et al., 2023), occurs concurrently with subsidence, including the formation of back-arc basins (Balázs et al., 2022; Larter et al., 2003). These geodynamic phenomena occur in close proximity, facilitating the orogenic collapse of the upper crust from uplifted regions to subsided ones.

In general, the evolution of extensional systems in these arcuate orogens varies depending on the involved geodynamic processes. While the extensional system in the central Betic Cordillera migrates in the same direction of the Gibraltar Arc, in other settings this is not the case. In the Banda Arc, the extension's migration is perpendicular to the subduction's migration (Pownall et al., 2013), and in the Scotia Arc, it is parallel but in the opposite direction (Morales-Ocaña et al., 2023). Furthermore, the model proposed here suggests that gravitational collapse can migrate, as seen during the Cenozoic in the Great Basin (Axen et al., 1993) or in the Tibetan Plateau, Himalaya (Guo et al., 2018), if the lithospheric processes generating them migrate in turn.

5. Conclusions

The normal VZF, responsible for the Mw 6.5 1884 catastrophic Andalusian earthquake, developed in the context of an active central Betic Cordillera in the framework of the Africa-Nubia convergence. The Zafarraya survey mode GNSS network determines that the development of the Sierra de Alhama-Zafarraya Polje area is related to a maximum NNE–SSW shortening of 2 mm/yr instead of the expected extension related to the normal VZF. The discrepancy between geological and GNSS data suggests the formation of the VZF is due to the bending-moment extension and collapse of the outer arc of the active Sierra de Alhama antiform. Its activity may be conditioned by the displacement on the basal detachment of the extensional system of the Granada Basin.

The Granada extensional system accommodates the W to SW-directed gravitational collapse driven by active uplift in the central Betic Cordillera and subsidence of the Western Alboran Basin due to the active rollback in the western Betic Cordillera. Seismicity indicates that the basal detachment of this system extends into the Sierra de Alhama-Zafarraya area. This area is part of an active compressional front extending from west of Sierra

Gorda to Sierra Tejeda in the SW of the Granada Basin. Development of the compressional front of the extensional collapse was favored by crustal heterogeneities and can be divided into two sectors. The northwestern one, located in the External Zones, is affected by thrusting. The southern sector, in the Internal Zones, is affected by folding and buttressing produced by a high-density crustal body.

The normal seismogenic VZF, having developed in the compressional front of the extensional system of the Granada Basin, constitutes a natural case study that sheds novel light on the complex interaction of extension and compression, faults, and folds, taking place in active orogens. A fuller understanding of the heterogeneous behavior of active tectonics driven by inherited structures is essential to ensure progress in future seismic hazard studies.

Data Availability Statement

Seismicity data can be found in the IGN online database (National Geographic Institute, 2023). The relocated seismicity data is available in Table S1 and are archived into Zenodo repository (Madarieta-Txurruka, González-Castillo, et al., 2023). Earthquake focal mechanisms are compiled in Table S2, sourced from both the literature and the IGN online database (SMT, 2023). Stress tensor calculation parameters are available in Table S3. Position time series of Zafarraya GNSS network are provided in Figure S1 and archived into Zenodo repository (Madarieta-Txurruka, González-Castillo, et al., 2023). Additionally, the DTMs used in geological maps were obtained from the CNIG (IGN) repository (CNIG, 2023).

Acknowledgments

The authors express their gratitude to two anonymous reviewers for their valuable input, which contributed to enhancing the quality of the article. They also extend their thanks to Dr. Taylor Schildgen and Dr. Luca Dal Zilio for their editorial management of the manuscript. The authors would also like to thank Angel Carlos López Garrido, Sergio Blanca, and Antonio Herrera for their help with GNSS surveys. This study was supported by BARACA (PID2022-136678NB-I00 AEI/FEDER, UE), P18-RT-3275, B-RNM-301-UGR18 (Junta de Andalucía/FEDER); Programa Operativo FEDER Andalucía 2014–2020 Ref. 126344 (University of Jaén); POAIUJA 2023/2024 (University of Jaén); Andalusian research groups RNM-148, RNM-282, and RNM-370. Funding for open access charge: Universidad de Granada / CBUA.

References

ABEM. (2006). *Instruction manual terrameter SAS 4000/SAS 1000*. ABEM Instrument AB.

Alonso-Chaves, F. M., & Orozco, M. (2007). Evolución tectónica de las Sierras de Tejeda y Almijara: Colapso extensional y exhumación de áreas metamórficas en el dominio de Alborán (Cordilleras Béticas). *Revista de la Sociedad Geologica de Espana*, *20*(3–4), 211–228.

Amrouch, K., Lacombe, O., Bellahsen, N., Daniel, J. M., & Callot, J. P. (2010). Stress and strain patterns, kinematics and deformation mechanisms in a basement-cored anticline: Sheep Mountain Anticline, Wyoming. *Tectonics*, *29*(1). https://doi.org/10.1029/2009TC002525

Axen, G. J., Taylor, W. J., & Bartley, J. M. (1993). Space-time patterns and tectonic controls of Tertiary extension and magmatism in the Great Basin of the western United States. *Geological Society of America Bulletin*, *105*(1), 56–76. https://doi.org/10.1130/0016-7606(1993)105%3C0056:STPATC%3E2.3.CO;2

Ayala, C., Bohoyo, F., Maestro, A., Reguera, M. I., Torne, M., Rubio, F., et al. (2016). Updated Bouguer anomalies of the Iberian Peninsula: A new perspective to interpret the regional geology. *Journal of Maps*, *12*(5), 1089–1092. https://doi.org/10.1080/17445647.2015.1126538

Balanyá, J. C., Crespo Blanc, A., Díaz Aspiroz, M., Expósito, I., Torcal, F., Pérez-Peña, V., et al. (2012). Arc-parallel vs. back-arc extensión in the Western Gibraltar Arc: Is the Gibraltar forearc still active? *Geológica Acta*, *10*, 249–263. https://doi.org/10.1344/105.000001771

Balanyá, J. C., & García-Dueñas, V. (1987). Les directions structurales dans le Domaine d'Alborán de part et d'autre du Détroit de Gibraltar. *Comptes rendus de l'Académie des sciences. Série 2, Mécanique, Physique, Chimie, Sciences de l'univers, Sciences de la Terre*, *304*(15), 929–932.

Balázs, A., Faccenna, C., Gerya, T., Ueda, K., & Funiciello, F. (2022). The dynamics of forearc–back-arc basin subsidence: Numerical models and observations from mediterranean subduction zones. *Tectonics*, *41*(5), e2021TC007078. https://doi.org/10.1029/2021TC007078

Banda, E., & Ansorge, J. (1980). Crustal structure under the central and eastern part of the Betic Cordillera. *Geophysical Journal International*, *63*(2), 515–532. https://doi.org/10.1111/j.1365-246X.1980.tb02635.x

Banda, E., Gallart, J., García-Dueñas, V., Dañobeitia, J. J., & Makris, J. (1993). Lateral variation of the crust in the Iberian peninsula: New evidence from the Betic Cordillera. *Tectonophysics*, *221*(1), 53–66. https://doi.org/10.1016/0040-1951(93)90027-H

Barker, P. F. (2001). Scotia Sea regional tectonic evolution: Implications for mantle flow and palaeocirculation. *Earth-Science Reviews*, *55*(1–2), 1–39. https://doi.org/10.1016/S0012-8252(01)00055-1

Bertiger, W., Bar-Sever, Y., Dorsey, A., Haines, B., Harvey, N., Hemberger, D., et al. (2020). GipsyX/RTGx, a new tool set for space geodetic operations and research. *Advances in Space Research*, *66*(3), 469–489. https://doi.org/10.1016/j.asr.2020.04.015

Bezzeghoud, M., Borges, J. F., & Caldeira, B. (2012). *Fontes sísmicas Ao Longo Da Fronteira de Placas tectónicas Entre Os Açores E a Argélia: Um Modelo sismotectónico*. Escolar Editora (volume Geologia de Portugal. chapter III.9).

Bilham, R., Larson, K., & Freymueller, J. (1997). GPS measurements of present-day convergence across the Nepal Himalaya. *Nature*, *386*(6620), 61–64. https://doi.org/10.1038/386061a0

Blanco, M. J., & Spakman, W. (1993). The P-wave velocity structure of the mantle below the Iberian Peninsula: Evidence for subducted lithosphere below southern Spain. *Tectonophysics*, *221*(1), 13–34. https://doi.org/10.1016/0040-1951(93)90025-F

Bleil, D. F. (1953). Induced polarization; a method of geophysical prospecting. *Geophysics*, *18*(3), 636–661. https://doi.org/10.1190/1.1437917

Borque, M. J., Galindo-Zaldívar, J., Gil, A. J., Jabaloy, A., Lacy, M. C., López, A. C., et al. (2005). Establishment of a non-permanent GPS network to monitor the deformation in Zafarraya Fault and Sierra Tejeda Antiform (Spain). *Física de la Tierra*, *17*, 23–31.

Boyer, S. E. (1995). Sedimentary basin taper as a factor controlling the geometry and advance of thrust belts. *American Journal of Science*, *295*(10), 1220–1254. https://doi.org/10.2475/ajs.295.10.1220

Braga, J. C., Martín, J. M., & Quesada, C. (2003). Patterns and average rates of late Neogene–Recent uplift of the Betic Cordillera, SE Spain. *Geomorphology*, *50*(1–3), 3–26. https://doi.org/10.1016/S0169-555X(02)00205-2

Brandes, C., & Tanner, D. C. (2014). Fault-related folding: A review of kinematic models and their application. *Earth-Science Reviews*, *138*, 352–370. https://doi.org/10.1016/j.earscirev.2014.06.008

Buck, W. R. (1988). Flexural rotation of normal faults. *Tectonics*, *7*(5), 959–973. https://doi.org/10.1029/TC007i005p00959

Buforn, E., Bezzeghoud, M., Udías, A., & Pro, C. (2004). Seismic sources on the Iberia-African Plate boundary and their tectonic implications. *Pure and Applied Geophysics*, *161*(3), 623–646. https://doi.org/10.1007/s00024-003-2466-1

Burchfiel, B. C., & Royden, L. H. (1985). North-south extension within the convergent Himalayan region. *Geology*, *13*(10), 679–682. https://doi.org/10.1130/0091-7613(1985)13%3C679:NEWTCH%3E2.0.CO;2

Calvert, A., Sandvol, E., Seber, D., Barazangi, M., Vidal, F., Alguacil, G., & Jabour, N. (2000). Propagation of regional seismic phases (Lg and Sn) and Pn velocity structure along the Africa–Iberia plate boundary zone: Tectonic implications. *Geophysical Journal International*, *142*(2), 384–408. https://doi.org/10.1046/j.1365-246x.2000.00160.x

Carmona, E., Stich, D., Ibañez, J. M., & Saccorotti, G. (2009). Multiplet focal mechanisms from polarities and relative locations: The Iznajar swarm in southern Spain. *Bulletin of the Seismological Society of America*, *99*(6), 3421–3429. https://doi.org/10.1785/0120090036

Chertova, M. V., Spakman, W., Geenen, T., Van Den Berg, A. P., & Van Hinsbergen, D. J. J. (2014). Underpinning tectonic reconstructions of the western Mediterranean region with dynamic slab evolution from 3-D numerical modeling. *Journal of Geophysical Research: Solid Earth*, *119*(7), 5876–5902. https://doi.org/10.1002/2014JB011150

CNIG. (2023). Download center of National Center of Geographic Information (CNIG). [Dataset]. IGN. Retrieved from http://centrodedescargas.cnig.es/CentroDescargas/

Cosgrove, J. W. (2015). The association of folds and fractures and the link between folding, fracturing and fluid flow during the evolution of a fold–thrust belt: A brief review. *Special Publications*, *421*(1), 41–68. https://doi.org/10.1144/SP421.11

Delph, J. R., Abgarmi, B., Ward, K. M., Beck, S. L., Özacar, A. A., Zandt, G., et al. (2017). The effects of subduction termination on the continental lithosphere: Linking volcanism, deformation, surface uplift, and slab tearing in central Anatolia. *Geosphere*, *13*(6), 1788–1805. https://doi.org/10.1130/GES01478.1

Delvaux, D., & Barth, A. (2010). African stress pattern from formal inversion of focal mechanism data. *Tectonophysics*, *482*(1–4), 105–128. https://doi.org/10.1016/j.tecto.2009.05.009

Delvaux, D., & Sperner, B. (2003). *New aspects of tectonic stress inversion with reference to the TENSOR program* (Vol. 212, pp. 75–100). Geological Society of London, Special Publication. https://doi.org/10.1144/GSL.SP.2003.212.01.06

DeMets, C., Gordon, R. G., & Argus, D. F. (2010). Geologically current plate motions. *Geophysical Journal International*, *181*(1), 1–80. https://doi.org/10.1111/j.1365-246X.2009.04491.x

Dewey, J. F. (1988). Extensional collapse of orogens. *Tectonics*, *7*(6), 1123–1139. https://doi.org/10.1029/TC007i006p01123

Diaz, J., Gallart, J., & Carbonell, R. (2016). Moho topography beneath the Iberian-Western Mediterranean region mapped from controlled-source and natural seismicity surveys. *Tectonophysics*, *692*, 74–85. https://doi.org/10.1016/j.tecto.2016.08.023

Do Couto, D., Gorini, C., Jolivet, L., Lebret, N., Augier, R., Gumiaux, C., et al. (2016). Tectonic and stratigraphic evolution of the Western Alborán Sea Basin in the last 25 Myrs. *Tectonophysics*, *677*, 280–311. https://doi.org/10.1016/j.tecto.2016.03.020

Douvillé, R. (1906). *La Peninsule Iberíque*, *III*(3), 1–175.

Elorza, J. J., García-Dueñas, V., González-Donoso, J. M., Martín García, L., & Matas Gónzalez, J. (1978). Mapa geológico de España a escala 1:50.000. Hoja número 1040 (Zafarraya).

England, P., & Houseman, G. (1989). Extension during continental convergence, with application to the Tibetan Plateau. *Journal of Geophysical Research*, *94*(B12), 17561–17579. https://doi.org/10.1029/JB094iB12p17561

England, P., & Molnar, P. (1997). Active deformation of Asia: From kinematics to dynamics. *Science*, *278*(5338), 647–650. https://doi.org/10.1126/science.278.5338.647

Fallot, P. (1948). Les cordilléres betiques. *Estudios Geológicos*, *4*, 259–279.

Fernández Fernández, E., Campos, J., & González Lodeiro, F. (1992). Estructuras extensionales en los materiales Aipujárrides al E de Málaga (Sierra Tejeda, Cordilleras Béticas). *Geogaceta*, *12*, 13–16.

Fernández-García, C., & Ruano, P. (2016). Caracterización de la geometría del Polje de Zafarraya a partir de prospección gravimétrica (Cordillera Bética). *Geogaceta*, *59*, 67–70.

Fillon, C., Huismans, R. S., van der Beek, P., & Muñoz, J. A. (2013). Syntectonic sedimentation controls on the evolution of the southern Pyrenean fold-and-thrust belt: Inferences from coupled tectonic-surface processes models. Journal of Geophysical Research. *Solid Earth*, *118*(10), 5665–5680. https://doi.org/10.1002/jgrb.50368

Flesch, L. M., Holt, W. E., Haines, A. J., & Shen-Tu, B. (2000). Dynamics of the Pacific-North American plate boundary in the western United States. *Science*, *287*(5454), 834–836. https://doi.org/10.1126/science.287.5454.834

Fontboté, J. M., & Estévez, A. (1980). *Geología de las Cordilleras Béticas* (pp. 91–92). Boletin Geologico y Minero.

Foster, D. A., Ma, C., Goscombe, B. D., & Mueller, P. A. (2023). Extensional collapse of orogens: A review and example from the Southern Appalachian orogen. In I. J. Catlos & I. Çemen (Eds.), *Compressional tectonics: Plate convergence to mountain building* (Vol. 1, pp. 301–319). https://doi.org/10.1002/9781119773856.ch12

Galindo-Zaldívar, J., Gil, A. J., Borque, M. J., González-Lodeiro, F., Jabaloy, A., Marín-Lechado, C., et al. (2003). Active faulting in the internal zones of the central Betic Cordilleras (SE, Spain). *Journal of Geodynamics*, *36*(1–2), 239–250. https://doi.org/10.1016/S0264-3707(03)00049-8

Galindo-Zaldívar, J., Gil, A. J., Sanz de Galdeano, C., de Lacy, M. C., García-Armenteros, J. A., Ruano, P., et al. (2015). Active shallow extension in central and eastern Betic Cordillera from CGPS data. *Tectonophysics*, *663*, 290–301. https://doi.org/10.1016/j.tecto.2015.08.035

Galindo-Zaldívar, J., Gil, A. J., Tendero-Salmerón, V., Borque, M. J., Ercilla, G., González-Castillo, L., et al. (2022). The Campo de Dalias GNSS network Unveils the interaction between Roll-back and Indentation tectonics in the Gibraltar Arc. *Sensors*, *22*(6), 2128. https://doi.org/10.3390/s22062128

Galindo-Zaldívar, J., González-Lodeiro, F., & Jabaloy, A. (1989). Progressive extensional shear structures in a detachment contact in the Western Sierra Nevada (Betic Cordilleras, Spain). *Geodinamica Acta*, *3*(1), 73–85. https://doi.org/10.1080/09853111.1989.11105175

Galindo-Zaldívar, J., González Lodeiro, F., & Jabaloy, A. (1993). Stress and palaeostress in the Betic-Rif cordilleras (Miocene to the present). *Tectonophysics*, *227*(1–4), 105–126. https://doi.org/10.1016/0040-1951(93)90090-7

Galindo-Zaldívar, J., Jabaloy, A., & González-Lodeiro, F. (1996). Reactivation du detachement extensif de Mecina dans le secteur occidental de la Sierra Nevada (Cordilleres Betiques, SE de l'Espagne). *Comptes Rendus de l'Academie des Sciences-Serie IIa-Sciences de la Terre et des Planetes*, *323*(7), 615–622.

Galindo-Zaldívar, J., Jabaloy, A., González-Lodeiro, F., & Aldaya, F. (1997). Crustal structure of the central sector of the Betic Cordillera (SE Spain). *Tectonics*, *16*(1), 18–37. https://doi.org/10.1029/96TC02359

Galindo-Zaldívar, J., Jabaloy, A., Serrano, I., Morales, J., González-Lodeiro, F., & Torcal, F. (1999). Recent and present-day stresses in the Granada Basin (Betic Cordilleras): Example of a late Miocene-present-day extensional basin in a convergent plate boundary. *Tectonics*, *18*(4), 686–702. https://doi.org/10.1029/1999TC900016

Galindo-Zaldívar, J., Ruano, P., Jabaloy, A., & López-Chicano, M. (2000). Kinematics of faults between Subbetic Units during the Miocene (central sector of the Betic Cordillera). *Comptes Rendus de l'Academie des Sciences - Series IIA: Earth and Planetary Science*, *331*(12), 811–816. https://doi.org/10.1016/S1251-8050(00)01484-1

Garcia-Castellanos, D., & Villaseñor, A. (2011). Messinian salinity crisis regulated by competing tectonics and erosion at the Gibraltar arc. *Nature*, *480*(7377), 359–363. https://doi.org/10.1038/nature10651

García-Jerez, A., Luzón, F., Navarro, M., & Pérez-Ruiz, J. A. (2006). Characterization of the sedimentary cover of the Zafarraya Polje, southern Spain, by means of ambient noise. *Bulletin of the Seismological Society of America*, *96*(3), 957–967. https://doi.org/10.1785/0120050061

Ghani, H., Sobel, E. R., Zeilinger, G., Glodny, J., Irum, I., & Sajid, M. (2021). Spatio-temporal structural evolution of the Kohat fold and thrust belt of Pakistan. *Journal of Structural Geology*, *145*, 104310. https://doi.org/10.1016/j.jsg.2021.104310

Gil, A. J., Galindo-Zaldívar, J., Borque, M. J., Marin-Lechado, C., Ruano, P., & de Galdeano, C. S. (2005). Geodetic deformation monitoring in Zafarraya Fault and Sierra Tejeda antiform (Spain): Status report. *Acta Geodynamica et Geromaterialia*, *2*(1), 25–29.

Gil, A. J., Galindo-Zaldívar, J., Sanz de Galdeano, C., Borque, M. J., Sánchez-Alzola, A., Martinez-Martos, M., & Alfaro, P. (2017). The Padul normal fault activity constrained by GPS data: Brittle extension orthogonal to folding in the central Betic Cordillera. *Tectonophysics*, *712*, 64–71. https://doi.org/10.1016/j.tecto.2017.05.008

Goldsworthy, M., & Jackson, J. (2001). Migration of activity within normal fault systems: Examples from the Quaternary of mainland Greece. *Journal of Structural Geology*, *23*(2–3), 489–506. https://doi.org/10.1016/S0191-8141(00)00121-8

González-Castillo, L., Galindo-Zaldivar, J., de Lacy, M. C., Borque, M. J., Martinez-Moreno, F. J., García-Armenteros, J. A., & Gil, A. J. (2015a). Active rollback in the Gibraltar Arc: Evidences from CGPS data in the western Betic Cordillera. *Tectonophysics*, *663*, 310–321. https://doi.org/10.1016/j.tecto.2015.03.010

González-Castillo, L., Galindo-Zaldívar, J., Pedrera, A., Martínez-Moreno, F. J., & Ruano, P. (2015b). Shallow frontal deformation related to active continental subduction: Structure and recent stresses in the westernmost Betic Cordillera. *Terra Nova*, *27*(2), 114–121. https://doi.org/10.1111/ter.12138

Gresseth, J. L. S., Osmundsen, P. T., & Péron-Pinvidic, G. (2023). 3D evolution of detachment fault systems in necking domains: Insights from the Klakk Fault Complex and the Frøya High, mid-Norwegian rifted margin. *Tectonics*, *42*(3), e2022TC007600. https://doi.org/10.1029/2022TC007600

Grützner, C., Ruano, P., Jabaloy, A., Galindo-Zaldívar, J., Becker-Heidmann, P., Sanz de Galdeano, C., et al. (2013). Late Holocene rupture history of the Ventas de Zafarraya Fault (Southern Spain). *Cuaternario y Geomorfologia*, *27*(3–4), 5–32.

Guo, X., Gao, R., Zhao, J., Xu, X., Lu, Z., Klemperer, S. L., & Liu, H. (2018). Deep-seated lithospheric geometry in revealing collapse of the Tibetan Plateau. *Earth-Science Reviews*, *185*, 751–762. https://doi.org/10.1016/j.earscirev.2018.07.013

Herraiz, M., De Vicente, G., Lindo, R., Giner, J., Simón, J. L., González Casado, J. M., et al. (1998). Proyecto Sigma. In *Análisis del estado de esfuerzos tectónicos reciente y actual en la Península Ibérica. Colección Otros Documentos* (Vol. 10). Cons. de Seguridad Nucl.

Hinsch, R., Krawczyk, C. M., Gaedicke, C., Giraudo, R., & Demuro, D. (2002). Basement control on oblique thrust sheet evolution: Seismic imaging of the active deformation front of the Central Andes in Bolivia. *Tectonophysics*, *355*(1–4), 23–39. https://doi.org/10.1016/S0040-1951(02)00132-4

Houseman, G. A., McKenzie, D. P., & Molnar, P. (1981). Convective instability of a thickened boundary layer and its relevance for the thermal evolution of continental convergent belts. *Journal of Geophysical Research*, *86*(B7), 6115–6132. https://doi.org/10.1029/JB086iB07p06115

Hreinsdóttir, S., Freymueller, J. T., Bürgmann, R., & Mitchell, J. (2006). Coseismic deformation of the 2002 Denali fault earthquake: Insights from GPS measurements. *Journal of Geophysical Research*, *111*(B3). https://doi.org/10.1029/2005JB003676

Jabaloy, A., Galindo-Zaldívar, J., & González-Lodeiro, F. (1993). The Alpujárride-Nevado-Fibábride extensional shear zone, Betic Cordillera, SE Spain. *Journal of Structural Geology*, *15*(3–5), 555–569. https://doi.org/10.1016/0191-8141(93)90148-4

Jackson, J. A. (1987). Active normal faulting and crustal extension. *Geological Society, London, Special Publications*, *28*(1), 3–17. https://doi.org/10.1144/GSL.SP.1987.028.01.02

Jackson, J. A., & White, N. J. (1989). Normal faulting in the upper continental crust: Observations from regions of active extension. *Journal of Structural Geology*, *11*(1–2), 15–36. https://doi.org/10.1016/0191-8141(89)90033-3

Jia, D., Li, Y., Yan, B., Li, Z., Wang, M., Chen, Z., & Zhang, Y. (2020). The Cenozoic thrusting sequence of the Longmen Shan fold-and-thrust belt, eastern margin of the Tibetan Plateau: Insights from low-temperature thermochronology. *Journal of Asian Earth Sciences*, *198*, 104381. https://doi.org/10.1016/j.jseaes.2020.104381

Keller, E. A., & Pinter, N. (1996). In *Active tectonics: Earthquakes uplift and landscapes* (Vol. 333). Prentice Hall.

Kouba, J. (2005). A possible detection of the 26 December 2004 Great Sumatra-Andaman Islands Earthquake with solution products of the International GNSS Service. *Studia Geophysica et Geodaetica*, *49*(4), 463–483. https://doi.org/10.1007/s11200-005-0022-4

Kreemer, C., Blewitt, G., & Klein, E. C. (2014). A geodetic plate motion and Global Strain Rate Model. *Geochemistry, Geophysics, Geosystems*, *15*(10), 3849–3889. https://doi.org/10.1002/2014GC005407

Larson, K. M., Lowry, A. R., Kostoglodov, V., Hutton, W., Sánchez, O., Hudnut, K., & Suárez, G. (2004). Crustal deformation measurements in Guerrero, Mexico. *Journal of Geophysical Research*, *109*(B4). https://doi.org/10.1029/2003JB002843

Larter, R. D., Vanneste, L. E., Morris, P., & Smythe, D. K. (2003). Structure and tectonic evolution of the South Sandwich arc. *Geological Society, London, Special Publications*, *219*(1), 255–284. https://doi.org/10.1144/GSL.SP.2003.219.01.13

Li, T., Chen, J., Thompson Jobe, J. A., Burbank, D. W., Cheng, X., Xu, J., et al. (2018). Active bending-moment faulting: Geomorphic expression, controlling conditions, Accommodation of Fold Deformation. *Tectonics*, *37*(8), 2278–2306. https://doi.org/10.1029/2018TC004982

Livio, F., Kettermann, M., Reicherter, K., & Urai, J. L. (2019). Growth of bending-moment faults due to progressive folding: Insights from sandbox models and paleoseismological implications. *Geomorphology*, *326*, 152–166. https://doi.org/10.1016/j.geomorph.2018.02.012

Loke, M. H. (2019). *Tutorial: 2-D and 3-D electrical imaging surveys*. Geotomo Software.

López Arroyo, A., Martín Martín, A. J., & Mezcua Rodríguez, J. (1980). Terremoto de Andalucía. Influencia en sus efectos de las condiciones del terreno y del tipo de construcción. El terremoto de Andalucía de 1884 (pp. 5–94).

López-Sánchez, C., Buforn, E., Cesca, S., Lozano, L., de Galdeano, C. S., Mattesini, M., et al. (2022). Intermediate-depth earthquakes in southern Spain and Alborán Sea. *Tectonophysics*, *825*, 229238. https://doi.org/10.1016/j.tecto.2022.229238

Lozano, L., Cantavella, J. V., Gaite, B., Ruiz-Barajas, S., Antón, R., & Barco, J. (2022). Seismic analysis of the 2020–2021 Santa Fe seismic sequence in the Granada Basin, Spain: Relocations and focal mechanisms. *Seismological Society of America*, *93*(6), 3246–3265. https://doi.org/10.1785/0220220097

Madarieta-Txurruka, A., Galindo-Zaldívar, J., González-Castillo, L., Peláez, J. A., Ruiz-Armenteros, A. M., Henares, J., et al. (2021). High-and low-angle Normal Fault activity in a Collisional Orogen: The Northeastern Granada Basin (Betic Cordillera). *Tectonics*, *40*(7), e2021TC006715. https://doi.org/10.1029/2021TC006715

Madarieta-Txurruka, A., González-Castillo, L., Peláez, J. A., Catalán, M., Henares, J., Gil, A. J., et al. (2022). The role of faults as barriers in confined seismic sequences: 2021 seismicity in the Granada Basin (Betic Cordillera). *Tectonics*, *41*(9), e2022TC007481. https://doi.org/10.1029/2022TC007481

Madarieta-Txurruka, A., González-Castillo, L., Peláez, J. A., Galindo-Zaldívar, J., Borque, M. J., de Lacy, M. C., et al. (2023). Dataset for Active shortening simultaneous to normal faulting based on GNSS, geophysical and geological data: The seismogenic Ventas de Zafarraya Fault (Betic Cordillera). Tectonics [Dataset]. Zenodo. https://doi.org/10.5281/zenodo.10423744

Madarieta-Txurruka, A., Peláez, J. A., González-Castillo, L., Gil, A. J., & Galindo-Zaldívar, J. (2023b). Active collapse in the central Betic Cordillera: Development of the extensional system of the Granada Basin. *Applied Sciences*, *13*(16), 9138. https://doi.org/10.3390/app13169138

Mancilla, F. L., Booth-Rea, G., Stich, D., Pérez-Peña, J. V., Morales, J., Azañón, J. M., et al. (2015). Slab rupture and delamination under the Betics and Rif constrained from receiver functions. *Tectonophysics*, *663*, 225–237. https://doi.org/10.1016/j.tecto.2015.06.028

Mancktelow, N. S., & Pavlis, T. L. (1994). Fold-fault relationships in low-angle detachment systems. *Tectonics*, *13*(3), 668–685. https://doi.org/10.1029/93TC03489

Martín, R., Stich, D., Morales, J., & Mancilla, F. (2015). Moment tensor solutions for the Iberian-Maghreb region during the IberArray deployment (2009–2013). *Tectonophysics*, *663*, 261–274. https://doi.org/10.1016/j.tecto.2015.08.012

Martínez-Martínez, J. M., Soto, J. I., & Balanyá, J. C. (2002). Orthogonal folding of extensional detachments: Structure and origin of the Sierra Nevada elongated dome (Betics, SE Spain). *Tectonics*, *21*(3), 3. https://doi.org/10.1029/2001TC001283

Martinez Solares, J. M., & Mezcua, J. (2002). *Catálogo sísmico de la Península Ibérica (880 a.C.-1900)*. Monografía número 18. Dirección General del Instituto Geográfico Nacional.

Martin-Rojas, I., Alfaro, P., Galindo-Zaldívar, J., Borque-Arancón, M. J., García-Tortosa, F. J., Sanz de Galdeano, C., et al. (2023). Insights of active extension within a collisional orogen from GNSS (Central Betic Cordillera, S Spain). *Tectonics*, *42*(7), e2022TC007723. https://doi.org/10.1029/2022TC007723

McCalpin, J. P. (1996). *Paleoseismology*. International Geophysics Series (Vol. 62). Academic Press.

McClusky, S., Reilinger, R., Mahmoud, S., Ben Sari, D., & Tealeb, A. (2003). GPS constraints on Africa (Nubia) and Arabia plate motions. *Geophysical Journal International*, *155*(1), 126–138. https://doi.org/10.1046/j.1365-246X.2003.02023.x

Meghraoui, M., & Doumaz, F. (1996). Earthquake-induced flooding and paleoseismicity of the El Asnam, Algeria, fault-related fold. *Journal of Geophysical Research*, *101*(B8), 17617–17644. https://doi.org/10.1029/96JB00650

Meighan, H. E., ten Brink, U., & Pulliam, J. (2013). Slab tears and intermediate-depth seismicity. *Geophysical Research Letters*, *40*(16), 4244–4248. https://doi.org/10.1002/grl.50830

Mezcua, J., Rueda, J., & García Blanco, R. M. (2004). Reevaluation of historic earthquakes in Spain. *Seismological Research Letters*, *75*(1), 75–81. https://doi.org/10.1785/gssrl.75.1.75

Mitra, G. (1997). Evolution of salients in a fold-and-thrust belt: The effects of sedimentary basin geometry, strain distribution and critical taper. In *Evolution of geological structures in micro-to macro-scales* (pp. 59–90). Springer.

Morales, J., Serrano, I., Jabaloy, A., Galindo-Zaldivar, J., Zhao, D., Torcal, F., et al. (1999). Active continental subduction beneath the Betic Cordillera and the Alborán Sea. *Geology*, *27*(8), 735–738. https://doi.org/10.1130/0091-7613(1999)027%3C0735:ACSBTB%3E2.3.CO;2

Morales, J., Vidal, F., De Miguel, F., Alguacil, G., Posadas, A. M., Ibáñez, J. M., et al. (1990). Basement structure of the Granada basin, Betic Cordilleras, southern Spain. *Tectonophysics*, *177*(4), 337–348. https://doi.org/10.1016/0040-1951(90)90394-N

Morales-Ocaña, C., Bohoyo, F., Escutia, C., Marín-Lechado, C., Rey-Moral, C., Druet, M., et al. (2023). 3D geophysical and geological modeling of the South Orkney Microcontinent (Antarctica): Tectonic implications for the Scotia Arc development. *Tectonics*, *42*(4), e2022TC007602. https://doi.org/10.1029/2022TC007602

Morley, C. K. (2007). Development of crestal normal faults associated with deepwater fold growth. *Journal of Structural Geology*, *29*(7), 1148–1163. https://doi.org/10.1016/j.jsg.2007.03.016

Moustafa, A. R. (2013). Fold-related faults in the Syrian Arc belt of northern Egypt. *Marine and Petroleum Geology*, *48*, 441–454. https://doi.org/10.1016/j.marpetgeo.2013.08.007

Mudarra-Hernández, M., Mosquera-Feijoo, J. C., & Sanz-Pérez, E. (2023). Numerical simulation and characterization of the Hydromechanical Alterations at the Zafarraya Fault due to the 1884 Andalusia Earthquake (Spain). *Water*, *15*(5), 850. https://doi.org/10.3390/w15050850

Nabavi, S. T., & Fossen, H. (2021). Fold geometry and folding–a review. *Earth-Science Reviews*, *222*, 103812. https://doi.org/10.1016/j.earscirev.2021.103812

National Geographic Institute. (2023). Spanish seismic catalog [Dataset]. Instituto Geografico Nacional. https://doi.org/10.7419/162.03.2022

Niemi, N. A., Wernicke, B. P., Friedrich, A. M., Simons, M., Bennett, R. A., & Davis, J. L. (2004). BARGEN continuous GPS data across the eastern Basin and Range province, and implications for fault system dynamics. *Geophysical Journal International*, *159*(3), 842–862. https://doi.org/10.1111/j.1365-246X.2004.02454.x

Nocquet, J. M., & Calais, E. (2003). Crustal velocity field of western Europe from permanent GPS array solutions, 1996–2001. *Geophysical Journal International*, *154*(1), 72–88. https://doi.org/10.1046/j.1365-246X.2003.01935.x

Nocquet, J. M., Sue, C., Walpersdorf, A., Tran, T., Lenôtre, N., Vernant, P., et al. (2016). Present-day uplift of the western Alps. *Scientific Reports*, *6*(1), 28404. https://doi.org/10.1038/srep28404

Ollero Robles, E., & García García, J. L. (1984). Morfología del sustrato y geometría del acuífero aluvial del polje de Zafarraya (Granada). In *I Congreso Español de Geología* (Vol. 4, pp. 307–315).

Ori, G. G., & Friend, P. F. (1984). Sedimentary basins formed and carried piggyback on active thrust sheets. *Geology*, *12*(8), 475–478. https://doi.org/10.1130/0091-7613(1984)12%3C475:SBFACP%3E2.0.CO;2

Palano, M., González, P. J., & Fernández, J. (2015). The diffuse plate boundary of Nubia and Iberia in the western Mediterranean: Crustal deformation evidence for viscous coupling and fragmented lithosphere. *Earth and Planetary Science Letters*, *430*, 439–447. https://doi.org/10.1016/j.epsl.2015.08.040

Palomeras, I., Thurner, S., Levander, A., Liu, K., Villasenor, A., Carbonell, R., & Harnafi, M. (2014). Finite-frequency Rayleigh wave tomography of the western Mediterranean: Mapping its lithospheric structure. *Geochemistry, Geophysics, Geosystems*, *15*(1), 140–160. https://doi.org/10.1002/2013GC004861

Parera-Portell, J. A., Mancilla, F. D. L., Almendros, J., Morales, J., & Stich, D. (2023). Slab tearing underneath the Bransfield strait, Antarctica. *Geophysical Research Letters*, *50*(13), e2023GL103813. https://doi.org/10.1029/2023GL103813

Pedrera, A., Ruiz-Constan, A., Galindo-Zaldívar, J., Chalouan, A., De Galdeano, C. S., Marín-Lechado, C., et al. (2011). Is there an active subduction beneath the Gibraltar orogenic arc? Constraints from Pliocene to present-day stress field. *Journal of Geodynamics*, *52*(2), 83–96. https://doi.org/10.1016/j.jog.2010.12.003

Pedrera, A., Ruiz-Constán, A., García-Senz, J., Azor, A., Marín-Lechado, C., Ayala, C., et al. (2020). Evolution of the South-Iberian paleomargin: From hyperextension to continental subduction. *Journal of Structural Geology*, *138*, 104122. https://doi.org/10.1016/j.jsg.2020.104122

Pérez-Peña, J. V., Azor, A., Azañón, J. M., & Keller, E. A. (2010). Active tectonics in the Sierra Nevada (Betic Cordillera, SE Spain): Insights from geomorphic indexes and drainage pattern analysis. *Geomorphology*, *119*(1–2), 74–87. https://doi.org/10.1016/j.geomorph.2010.02.020

Platt, J. P., Anczkiewicz, R., Soto, J. I., Kelley, S. P., & Thirlwall, M. (2006). Early Miocene continental subduction and rapid exhumation in the western Mediterranean. *Geology*, *34*(11), 981–984. https://doi.org/10.1130/G22801A.1

Platt, J. P., & Vissers, R. L. M. (1989). Extensional collapse of thickened continental lithosphere: A working hypothesis for the Alborán Sea and Gibraltar arc. *Geology*, *17*(6), 540–543. https://doi.org/10.1130/0091-7613(1989)017%3C0540:ECOTCL%3E2.3.CO;2

Pownall, J. M., Hall, R., & Watkinson, I. M. (2013). Extreme extension across Seram and Ambon, eastern Indonesia: Evidence for Banda slab rollback. *Solid Earth*, *4*(2), 277–314. https://doi.org/10.5194/se-4-277-2013

QAFI. (2023). Quaternary faults database of Iberia. Retrieved from https://info.igme.es/qafi/

Ramsay, J. G. (1967). *Folding and fracturing of rocks*. McGrawHill.

Ratschbacher, L., Frisch, W., Linzer, H. G., & Merle, O. (1991). Lateral extrusion in the Eastern Alps, part 2: Structural analysis. *Tectonics*, *10*(2), 257–271. https://doi.org/10.1029/90TC02623

Reicherter, K. R., Jabaloy, A., Galindo-Zaldívar, J., Ruano, P., Becker-Heidmann, P., Morales, J., et al. (2003). Repeated palaeoseismic activity of the Ventas de Zafarraya fault (S Spain) and its relation with the 1884 Andalusian earthquake. *International Journal of Earth Sciences*, *92*(6), 912–922. https://doi.org/10.1007/s00531-003-0366-3

Reinhardt, L. J., Dempster, T. J., Shroder, J. F., Jr., & Persano, C. (2007). Tectonic denudation and topographic development in the Spanish Sierra Nevada. *Tectonics*, *26*(3). https://doi.org/10.1029/2006TC001954

Rey, P., Vanderhaeghe, O., & Teyssier, C. (2001). Gravitational collapse of the continental crust: Definition, regimes and modes. *Tectonophysics*, *342*(3–4), 435–449. https://doi.org/10.1016/S0040-1951(01)00174-3

Rey, P. F., Mondy, L., Duclaux, G., Teyssier, C., Whitney, D. L., Bocher, M., & Prigent, C. (2017). The origin of contractional structures in extensional gneiss domes. *Geology*, *45*(3), 263–266. https://doi.org/10.1130/G38595.1

Rey, P. F., Teyssier, C., Kruckenberg, S. C., & Whitney, D. L. (2011). Viscous collision in channel explains double domes in metamorphic core complexes. *Geology*, *39*(4), 387–390. https://doi.org/10.1130/G31587.1

Rey, P. F., Teyssier, C., & Whitney, D. L. (2010). Limit of channel flow in orogenic plateaux. *Lithosphere*, *2*(5), 328–332. https://doi.org/10.1130/L114.1

Rodríguez, L. R., López, F., Oliveira, J. T., Medialdea, T., Terrinha, P., Matas, J., et al. (2015). Mapa Geológico de la Península Ibérica, Baleares y Canarias a escala 1:1.000.000, edición 2015. IGME, LNEG. Retrieved from http://info.igme.es/cartografiadigital/datos/geologicos1M/Geologico1000_(2015)/pdfs/EditadoG1000_(2015).pdf

Rodríguez-Fernández, J., & Sanz de Galdeano, C. (2006). Late orogenic intramontane basin development: The Granada basin, Betics (southern Spain). *Basin Research*, *18*(1), 85–102. https://doi.org/10.1111/j.1365-2117.2006.00284.x

Rodríguez Pascua, M. A. (1997). Paleosismicidad en emplazamientos nucleares. Estudio en relación con el cálculo de peligrosidad sísmica. In *Colección Otros Documentos*. CSN.

Rodríguez Pascua, M. A., & De Vicente, G. (2001). Estado de esfuerzos actual en la Cordillera Bética Oriental. *Boletin Geologico y Minero*, *112*(4), 79–95.

Rosenbaum, G., Lister, G. S., & Duboz, C. (2002). Reconstruction of the tectonic evolution of the western Mediterranean since the Oligocene. *Journal of the Virtual Explorer*, *8*(10.3809). https://doi.org/10.3809/jvirtex.2002.00053

Ruano, P. (2003). *Estructuras tectónicas recientes en la transversal central de las cordilleras béticas*. (Doctoral dissertation). Universidad de Granada.

Ruano, P., Galindo-Zaldívar, J., & Jabaloy, A. (2004). Recent tectonic structures in a transect of the Central Betic Cordillera. *Pure and Applied Geophysics*, *161*(3), 541–563. https://doi.org/10.1007/s00024-003-2462-5

Ruano, P., Gil, A. J., Galindo-Zaldívar, J., Rodríguez-Caderot, G., de Lacy, M. C., Ruiz-Armenteros, A. M., et al. (2011). Geodetic studies in the Zafarraya Fault (Betic Cordilleras). In C. Grützner, T. Fernández Steeger, I. Papanikolaou, K. Reicherter, P. G. Silva, R. Pérez-López, et al. (Eds.), *Earthquake geology and archaeology: Science, society and critical facilities*, *Proceedings volumen 2. 2nd INQUA-IGCP 567 international workshop on active tectonics, earthquake geology, archaeology and engineering, 19-24 September 2011, Corinth (Greece)*.

Ruiz-Constán, A., Galindo-Zaldívar, J., Pedrera, A., Celerier, B., & Marín-Lechado, C. (2011). Stress distribution at the transition from subduction to continental collision (northwestern and central Betic Cordillera). *Geochemistry, Geophysics, Geosystems*, *12*(12). https://doi.org/10.1029/2011GC003824

Ruiz-Constán, A., Stich, D., Galindo-Zaldívar, J., & Morales, J. (2009). Is the northwestern Betic Cordillera mountain front active in the context of the convergent Eurasia–Africa plate boundary? *Terra Nova*, *21*(5), 352–359. https://doi.org/10.1111/j.1365-3121.2009.00886.x

Sandwell, D. T., Garcia, E., Soofi, K., Wessel, P., & Smith, W. H. F. (2013). Towards 1 mGal global marine gravity from CryoSat-2, Envisat, and Jason-1. *The Leading Edge*, *32*(8), 892–899. https://doi.org/10.1190/tle32080892.1

Santos-Bueno, N., Fernández-García, C., Stich, D., Mancilla, F. d. L., Martín, R., Molina-Aguilera, A., & Morales, J. (2019). Focal mechanisms for subcrustal earthquakes beneath the Gibraltar Arc. *Geophysical Research Letters*, *46*(5), 2534–2543. https://doi.org/10.1029/2018GL081587

Sanz de Galdeano, C. (1985). La fracturación del borde sur de la depresión de Granada. (Discusión acerca del escenario del terremoto del 25-XII-1884). *Estudios Geológicos*, *41*(1–2), 59–68. https://doi.org/10.3989/egeol.85411-2690

Sanz de Galdeano, C. (1990). Geologic evolution of the Betic Cordilleras in the Western Mediterranean, Miocene to the present. *Tectonophysics*, *172*(1–2), 107–119. https://doi.org/10.1016/0040-1951(90)90062-D

Sanz de Galdeano, C. (2013). The Zafarraya Polje (Betic Cordillera, Granada, Spain), a basin open by lateral displacement and bending. *Journal of Geodynamics*, *64*, 62–70. https://doi.org/10.1016/j.jog.2012.10.004

Sanz de Galdeano, C., & Alfaro, P. (2004). Tectonic significance of the present relief of the Betic Cordillera. *Geomorphology*, *63*(3–4), 175–190. https://doi.org/10.1016/j.geomorph.2004.04.002

Sanz de Galdeano, C. S., Peláez, J. A., & López-Casado, C. (2003). Seismic potential of the main active faults in the Granada Basin (southern Spain). *Pure and Applied Geophysics*, *160*(8), 1537–1556. https://doi.org/10.1007/s00024-003-2359-3

Searle, M. P., & Lamont, T. N. (2020). Compressional metamorphic core complexes, low-angle normal faults and extensional fabrics in compressional tectonic settings. *Geological Magazine*, *157*(1), 101–118. https://doi.org/10.1017/S0016756819000207

Seber, D., Barazangi, M., Ibenbrahim, A., & Demnati, A. (1996). Geophysical evidence for lithospheric delamination beneath the Alborán Sea and Rif–Betic mountains. *Nature*, *379*(6568), 785–790. https://doi.org/10.1038/379785a0

Selverstone, J. (2005). Are the Alps collapsing? *Annual Review of Earth and Planetary Sciences*, *33*(1), 113–132. https://doi.org/10.1146/annurev.earth.33.092203.122535

Serpelloni, E., Vannucci, G., Pondrelli, S., Argnani, A., Casula, G., Anzidei, M., et al. (2007). Kinematics of the Western Africa-Eurasia plate boundary from focal mechanisms and GPS data. *Geophysical Journal International*, *169*(3), 1180–1200. https://doi.org/10.1111/j.1365-246X.2007.03367.x

Serrano, I. (1999). *Distribución espacial de la sismicidad en las Cordilleras Béticas-Mar de Alborán*. (Doctoral dissertation). University of Granada.

Silliphant, L. J., Engelder, T., & Gross, M. R. (2002). The state of stress in the limb of the Split Mountain anticline, Utah: Constraints placed by transected joints. *Journal of Structural Geology*, *24*(1), 155–172. https://doi.org/10.1016/S0191-8141(01)00055-4

Smith, K. D., von Seggern, D., Blewitt, G., Preston, L., Anderson, J. G., Wernicke, B. P., & Davis, J. L. (2004). Evidence for deep magma injection beneath Lake Tahoe, Nevada-California. *Science*, *305*(5688), 1277–1280. https://doi.org/10.1126/science.1101304

SMT. (2023). Seismic moment tensor [Dataset]. Instituto Geografico Nacional. Retrieved from https://www.ign.es/web/ign/portal/tensor-momento-sismico/

Spakman, W., & Hall, R. (2010). Surface deformation and slab–mantle interaction during Banda arc subduction rollback. *Nature Geoscience*, *3*(8), 562–566. https://doi.org/10.1038/ngeo917

Stephenson, B. J., Koopman, A., Hillgartner, H., McQuillan, H., Bourne, S., Noad, J. J., & Rawnsley, K. (2007). Structural and stratigraphic controls on fold-related fracturing in the Zagros Mountains, Iran: Implications for reservoir development. *Geological Society, London, Special Publications*, *270*(1), 1–221. https://doi.org/10.1144/GSL.SP.2007.270.01.01

Stich, D., Ammon, C. J., & Morales, J. (2003). Moment tensor solutions for small and moderate earthquakes in the Ibero-Maghreb region. *Journal of Geophysical Research*, *108*(B3). https://doi.org/10.1029/2002JB002057

Stich, D., Martín, R., & Morales, J. (2010). Moment tensor inversion for Iberia-Maghreb earthquakes 2005-2008. *Tectonophysics*, *483*(3–4), 390–398. https://doi.org/10.1016/j.tecto.2009.11.006

Šumi, F. (1965). Prospecting for non-metallic minerals by induced polarization. *Geophysical Prospecting*, *13*(4), 603–616. https://doi.org/10.1111/j.1365-2478.1965.tb01952.x

Tavani, S., Storti, F., Lacombe, O., Corradetti, A., Muñoz, J. A., & Mazzoli, S. (2015). A review of deformation pattern templates in foreland basin systems and fold-and-thrust belts: Implications for the state of stress in the frontal regions of thrust wedges. *Earth-Science Reviews*, *141*, 82–104. https://doi.org/10.1016/j.earscirev.2014.11.013

Torné, M., Banda, E., García-Duen, V., & Balanyá, J. C. (1992). Mantle-lithosphere bodies in the Alborán crustal domain (Ronda peridotites, Betic-Rif orogenic belt). *Earth and Planetary Science Letters*, *110*(1–4), 163–171. https://doi.org/10.1016/0012-821X(92)90046-X

Torné, M., Fernández, M., Comas, M. C., & Soto, J. I. (2000). Lithospheric structure beneath the Alborán Basin: Results from 3D gravity modeling and tectonic relevance. *Journal of Geophysical Research*, *105*(B2), 3209–3228. https://doi.org/10.1029/1999JB900281

Tricart, P., Torelli, L., Argnani, A., Rekhiss, F., & Zitellini, N. (1994). Extensional collapse related to compressional uplift in the Alpine Chain off northern Tunisia (Central Mediterranean). *Tectonophysics*, *238*(1–4), 317–329. https://doi.org/10.1016/0040-1951(94)90062-0

Tsukahara, K., & Takada, Y. (2018). Aseismic fold growth in southwestern Taiwan detected by InSAR and GNSS. *Earth Planets and Space*, *70*, 1–7. https://doi.org/10.1186/s40623-018-0816-6

Udías, A., & Muñoz, D. (1979). The Andalusian earthquake of 25 December 1884. *Tectonophysics*, *53*(3–4), 291–299. https://doi.org/10.1016/0040-1951(79)90074-X

van de Lagemaat, S. H., Swart, M. L., Vaes, B., Kosters, M. E., Boschman, L. M., Burton-Johnson, A., et al. (2021). Subduction initiation in the Scotia Sea region and opening of the Drake Passage: When and why? *Earth-Science Reviews*, *215*, 103551. https://doi.org/10.1016/j.earscirev.2021.103551

Van Hinsbergen, D. J., Vissers, R. L., & Spakman, W. (2014). Origin and consequences of western Mediterranean subduction, rollback, and slab segmentation. *Tectonics*, *33*(4), 393–419. https://doi.org/10.1002/2013tc003349

Vannucci, G., & Gasperini, P. (2004). The new release of the database of Earthquake Mechanisms of the Mediterranean Area (EMMA version 2). *Annals of Geophysics*, *47*, 307–334.

Vidal, F. (1986). *Sismotectónica de la región Béticas-Mar de Alborán*. Tesis Doctoral. Universidad de Granada.

Waldhauser, F. (2001). HypoDD: A computer program to compute double-difference earthquake locations. https://doi.org/10.7916/D8SN072H

Waldhauser, F., & Ellsworth, W. L. (2000). A double-difference earthquake location algorithm: Method and application to the Northern Hayward Fault, California. *Bulletin of the Seismological Society of America*, *90*(6), 1353–1368. https://doi.org/10.1785/0120000006

Wallace, R. E. (1987). Grouping and migration of surface faulting and variations in slip rates on faults in the Great Basin province. *Bulletin of the Seismological Society of America*, *77*(3), 868–876. https://doi.org/10.1785/BSSA0770030868

Watkins, H., Healy, D., Bond, C. E., & Butler, R. W. (2018). Implications of heterogeneous fracture distribution on reservoir quality; an analogue from the Torridon Group sandstone, Moine Thrust Belt, NW Scotland. *Journal of Structural Geology*, *108*, 180–197. https://doi.org/10.1016/j.jsg.2017.06.002

Wdowinski, S., & Axen, G. J. (1992). Isostatic rebound due to tectonic denudation: A viscous flow model of a layered lithosphere. *Tectonics*, *11*(2), 303–315. https://doi.org/10.1029/91TC02341

Wells, D. L., & Coppersmith, K. J. (1994). New empirical relationships among magnitude, rupture length, rupture width, rupture area, and surface displacement. *Bulletin of the Seismological Society of America*, *84*(4), 974–1002. https://doi.org/10.1785/BSSA0840040974

Wiltschko, D., & Eastman, D. (1983). *Role of basement warps and faults in localizing thrust fault ramps* (Vol. 158, pp. 177–190). Geological Society of America Memoir. https://doi.org/10.1130/MEM158-p177

Woodward, N. B. (1988). Regional structural and geophysical studies of interaction and Overlap—Primary and secondary basement controls on thrust sheet geometries. In C. J. Schmidt & W. J. Perry (Eds.), *Interaction of the Rocky mountain Foreland and the Cordilleran Thrust Belt*. https://doi.org/10.1130/MEM171

Wortel, M. J. R., & Spakman, W. (2000). Subduction and slab detachment in the Mediterranean-Carpathian region. *Science*, *290*(5498), 1910–1917. https://doi.org/10.1126/science.290.5498.1910

Yeats, R. S., Clark, M. N., Keller, E. A., & Rockwell, T. K. (1981). Active fault hazard in southern California: Ground rupture versus seismic shaking. *Geological Society of America Bulletin*, *92*(4), 189–196. https://doi.org/10.1130/0016-7606(1981)92%3C189:AFHISC%3E2.0.CO;2

Zeck, H. P., & Whitehouse, M. J. (1999). Hercynian, Pan-African, Proterozoic and Archean ion-microprobe zircon ages for a Betic-Rif core complex, Alpine belt, W Mediterranean--Consequences for its PTt path. *Contributions to Mineralogy and Petrology*, *134*(2–3), 134–149. https://doi.org/10.1007/s004100050474

Zhao, L., Fang, C., Xu, X., & Deng, P. (2022). Physical simulation experiments of structural deformation and hydrocarbon accumulation in piggyback thrust wedges. *Geological Journal*, *57*(9), 3558–3568. https://doi.org/10.1002/gj.4487

Zumberge, J. F., Heflin, M. B., Jefferson, D. C., Watkins, M. M., & Webb, F. H. (1997). Precise point positioning for the efficient and robust analysis of GPS data from large networks. *Journal of Geophysical Research*, *102*(B3), 5005–5017. https://doi.org/10.1029/96JB03860